Resolution of quantum and classical ghost imaging

Milena D'Angelo,* Alejandra Valencia, Morton H. Rubin, and Yanhua Shih
Department of Physics, University of Maryland at Baltimore County, Baltimore, Maryland 21250, USA
(Received 15 September 2004; published 14 July 2005)

The quantum ghost imaging phenomena, experimentally demonstrated a decade ago, exploited the apparent spooky action at a distance of entangled photon pairs and offered a novel approach toward imaging. Can ghost imaging effects be produced by "classical" light sources, such as separable systems of photon pairs or thermal light? If so, can these sources achieve the same accuracy achieved by entangled states? In order to answer these questions, we formulate the different physics behind entangled and separable systems in terms of a set of inequalities derived from the historical argument of Einstein, Podolsky, and Rosen. We show that the ghost images produced by separable sources are subject to the standard statistical limitations. However, entangled states offer the possibility of overcoming such limitations. Imaging can, therefore, achieve its fundamental limit through the high spatial resolution and nonlocal behavior of entangled systems.

DOI: 10.1103/PhysRevA.72.013810 PACS number(s): 42.50.Dv, 03.65.Ud, 42.50.St, 42.50.Ar

I. INTRODUCTION

The concept of imaging is well defined in classical optics. Based on geometrical optics, the stigmatic *image* of an object is produced by a lens in the plane defined by the Gaussian thin-lens equation

$$\frac{1}{s_i}+\frac{1}{s_o}=\frac{1}{f},$$

where s_o is the distance between object and lens, f is the focal length of the lens, and s_i is the distance between lens and image plane. As depicted in Fig. 1(a), the characteristic property of a lens (or other image forming system) is the ability to generate a one-to-one relationship between points of the object and image planes. All different momenta passing through a point of the object are collected by the lens into a point of the image plane. Such a point-to-point relationship ceases to exist when no lens (or other image forming system) is present, as depicted in Fig. 1(b). The optical effects obtained in such a case [Fig. 1(b)] is known as *projection*.

In practice, the point-to-point relationship drawn in Fig. 1(a) is affected by diffraction and transformed into a point-to-"spot" relationship. The width of the "spot" represents the *resolution* of the image and *is strictly related to the finite size of the imaging lens* (or, more precisely, to its numerical aperture). The spot is determined by the point-spread function which, for circular apertures (lenses or stops), is described by the function $P(\xi)=2J_1(\pi\xi)/(\pi\xi)$. The distance between the central maximum and the first minimum of this function represents the *diffraction limit*.

In the mid-1990s several experiments realized by our group proved the possibility of reproducing these well-known imaging effects in a nonlocal fashion [1–3], by employing entangled photon pairs and counting coincidences between two distant photon counting detectors. These effects were named quantum ghost interference [1] and quantum ghost image [2]. A schematic version of the unfolded setup for observing quantum ghost images is shown in Fig. 2. Differently from the classical imaging setup of Fig. 1, the source is placed in the middle: a pair of photons is emitted with all possible momenta and in all possible directions; however, if one photon is measured to have a certain transverse momentum, the transverse momentum of the other one is immediately known: it is equal but opposite. It is very surprising that although both detectors show fairly constant counting rates when scanned in the transverse plane, a point-to-point relationship arises between object and the image planes. A ghost image of the object is reproduced by counting coincidences between the two distant detectors, whenever the "two-photon Gaussian thin-lens equation" is satisfied [2]. Furthermore, a

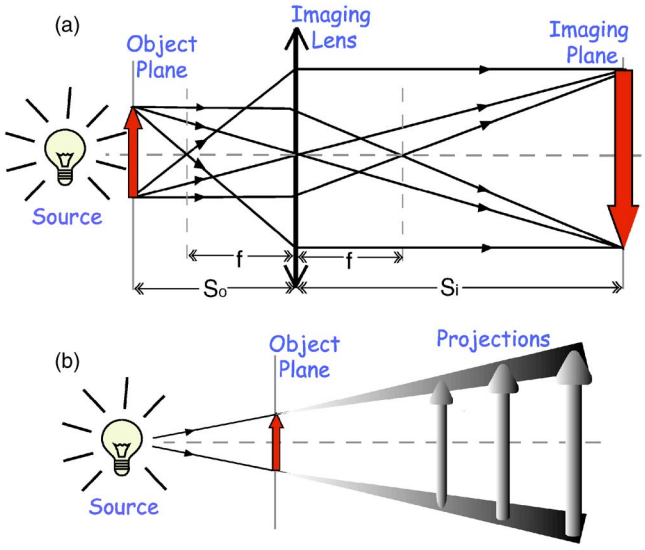

FIG. 1. (Color online) (a) A lens produces the stigmatic *image* of an object in the plane defined by the Gaussian thin-lens equation $1/s_i+1/s_o=1/f$. The concept of image is based on the existence of a point-to-point relationship between the object plane and the image plane. (b) A light source illuminates an object and no image forming system is present; no image plane is defined: only projections, or shadows, of the object can be observed.

*Electronic address: dmilena1@umbc.edu

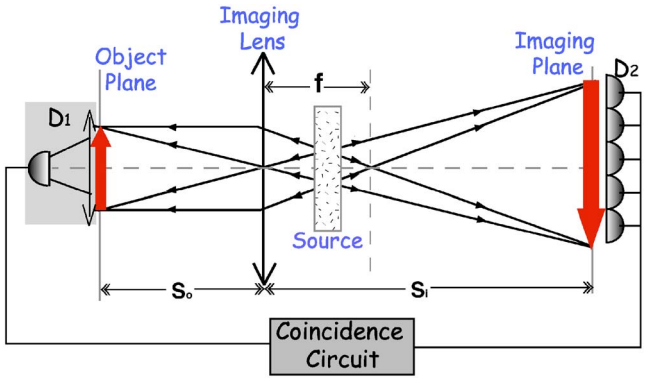

FIG. 2. (Color online) Schematic setup to observe a quantum ghost image. The source emits a pair of photons in all possible directions but their momenta are always equal and opposite (note the arrows on the "straight lines"). Object and imaging lens are inserted on one side of the source; a ghost image appears when counting coincidences between the fix bucket detector D_1 and the scanning pointlike detector D_2. The image plane is defined by the two-photon thin-lens equation $1/S_i+1/S_o=1/f$.

ghost interference-diffraction pattern [1] can be observed by placing the scanning detector in the focal plane of the imaging lens, as proposed by Klyshko [4].

Notice that the "straight lines" of Fig. 2 are the result of a perfect momentum-momentum two-photon correlation; they are physically different from the standard momenta depicted in Fig. 1. For instance, even an infinite imaging lens would not guarantee the perfect straight lines of Fig. 2 and, consequently, would not necessarily produce a ghost image. The quantum ghost image is the result of position-position two-photon correlation. In fact, the stigmatic ghost image drawn in Fig. 2 is affected by two essentially different mechanisms: (1) standard diffraction, due to the finite dimension of the lens, and (2) lack of perfect momentum-momentum two-photon correlation. This paper mainly focuses on the role played by this second point in ghost imaging effects.

The nonlocal nature of quantum ghost imaging has attracted a great deal of attention for practical applications. For instance, quantum metrology [5] is based on high-accuracy nonlocal positioning technology. Quantum lithography [6,7], on the other hand, represents a step forward with respect to quantum ghost imaging: *in the adequate experimental setup*, entangled two-photon systems can overcome the Rayleigh diffraction limit and generate superresolved images.

From a fundamental point of view, the interesting aspect of quantum ghost imaging resides in its strong connection with the original arguments of both Einstein, Polosky, and Rosen (EPR) [8] and Popper [9]. Quantum ghost image and interference effects can indeed be considered as the experimental manifestations of the historical EPR *gedankenexperiment*. It is in this perspective that Popper's experiment [10] and the experimental verification of the "EPR inequalities" have been realized [11], using entangled two-photon systems emitted by spontaneous parametric down-conversion (SPDC) [12].

Recently Bennink *et al.* [13] raised the question whether or not quantum ghost imaging effects could be reproduced "classically"—i.e., without entanglement. This work opened an intense debate which has been accompanied by both theoretical [14–16] and experimental [11,17] developments. For instance, Gatti *et al.* [16] suggested that, in a given setup, only entangled sources offer the possibility of reproducing both the ghost image and the ghost interference diffraction patterns of an object, whereas separable systems of photon pairs can only reproduce one of these effects. In a later work [18] the same authors, developing the idea presented in [19], proposed thermal light as a candidate for mimicking quantum ghost imaging effects. Interesting theoretical [20,21] and experimental [22–24] works have followed.

In this paper, we wish to reconcile these later developments with the original argument of EPR and to quantitatively compare quantum and classical ghost imaging [25]. In particular, we will focus on the fundamental limits of ghost measurements performed on both entangled and separable sources of photons.

We start by formulating the different physics behind entangled and separable systems of pairs of quanta in terms of the EPR inequalities (Sec. II). The EPR inequalities represent the key to identify the practical implications of entangled two-particle systems: entanglement offers the unique advantage of overcoming the limitations imposed by the uncertainty relations on separable systems. In Sec. III, we propose an operational approach for defining the measurements of momentum and position on systems of photons. The operational approach is then employed to identify the setup for implementing both EPR and Popper's thought experiments on systems of photon pairs. In Sec. IV, we predict the results of both EPR and Poppers's experiments performed on SPDC entangled two-photon systems. This analysis explicitly demonstrates the interesting practical implications of entangled two-photon systems: high-accuracy nonlocal positioning. In Secs. V and VI, we evaluate the results of coincidence experiments realized in the same experimental setups, when two different "classical" sources are employed [25]. In particular, in Sec. V, we consider a separable system of photon pairs characterized by classical statistical correlation in momentum, while, in Sec. VI, we consider a thermal source. The comparison of the results obtained for the three different sources proves that only quantum ghost imaging can go beyond the classical limitations.

II. ENTANGLED VERSUS SEPARABLE SYSTEMS

A. Two-particle entangled systems

Let us consider the following pure state describing a two-particle system entangled in momentum variables (p_1,p_2):

$$|\Psi^{(A)}\rangle_{12}=\int\int_{-\infty}^{+\infty}dp_1dp_2\tilde{A}(p_1+p_2)\tilde{C}\left(\frac{p_1-p_2}{2}\right)|p_1p_2\rangle, \tag{1}$$

with the assumption that the standard deviation (σ_A) *of* $\tilde{A}$ *is much smaller than the standard deviation* (σ_C) *of* $\tilde{C}$. This last condition implies that the entangled state of Eq. (1) is predominantly anticorrelated in momentum [as emphasized by the superscript (A)]. The probability amplitudes associated

with the entangled state of Eq. (1) in both the position and momentum representations are, respectively,

$$F(x_1,x_2) = \frac{1}{2\pi\hbar}\int\int_{-\infty}^{+\infty} dp_1 dp_2 \tilde{A}(p_1+p_2) \times \tilde{C}\left(\frac{p_1-p_2}{2}\right) e^{ip_1x_1/\hbar} e^{ip_2x_2/\hbar} = A\left(\frac{x_1+x_2}{2}\right) C(x_1-x_2),$$

$$\tilde{F}(p_1,p_2) = \tilde{A}(p_1+p_2)\tilde{C}\left(\frac{p_1-p_2}{2}\right); \quad (2)$$

i.e., they both factor in the variables (x_1+x_2, x_1-x_2) and (p_1+p_2, p_1-p_2), respectively. Equations (2) indicate that the two-particle probability amplitudes $F(x_1,x_2)$ and $\tilde{F}(p_1,p_2)$ are related to each other by two-dimensional (2D) Fourier transformation. This is a characteristic property of any two-particle entangled system. Furthermore, for the case considered here [Eq. (1)], the composing functions are related to each other by 1D Fourier transformation: $\tilde{A}(p_1+p_2)$ is the Fourier transform of $A((x_1+x_2)/2)$, and $\tilde{C}((p_1-p_2)/2)$ is the Fourier transform of $C(x_1-x_2)$. Both $(p_1+p_2, (x_1+x_2)/2)$ and $((p_1-p_2)/2, x_1-x_2)$ are pairs of Fourier-conjugate variables. However, since (x_1-x_2) and (p_1+p_2) are not Fourier-conjugate variables, the two-particle probability distributions $|F(x_1,x_2)|^2$ and $|\tilde{F}(p_1,p_2)|^2$ may give rise to independent minimum uncertainties—i.e.,

$$\Delta(p_1+p_2) = \sigma_A \ll \Delta p_{1,2},$$

$$\Delta(x_1-x_2) = \frac{\hbar}{\sigma_C} \ll \Delta x_{1,2}, \quad (3)$$

where $\Delta p_{1,2} = 1/2\sqrt{\sigma_A^2+\sigma_C^2}$ and $\Delta x_{1,2} = \hbar/(2\sigma_A\sigma_C)\sqrt{\sigma_A^2+\sigma_C^2}$ are the minimum uncertainties associated with each particle of the entangled system. The minimum uncertainties σ_A and $\hbar/\sigma_C$ correspond to the case of Gaussian probability distributions $|A|^2$ and $|C|^2$, respectively. Equations (3) indicate that, even if the uncertainties $\Delta p_{1,2}$ and $\Delta x_{1,2}$ are quite large, the uncertainties in both $\Delta(p_1+p_2)$ and $\Delta(x_1-x_2)$ can be indefinitely small. Based on the results of both Eqs. (2) and (3), we conclude that entangled two-particle states may give rise to *completely independent uncertainties for total momentum* (p_1+p_2) *and relative position* (x_1-x_2): the increase or decrease of one does not affect, in any way, the other.

The independence between $\Delta(p_1+p_2)$ and $\Delta(x_1-x_2)$ is even more striking when considering the original EPR two-particle system [8]

$$|\Psi\rangle_{EPR} = \int\int_{-\infty}^{+\infty} dp_1 dp_2 \delta(p_1+p_2)|p_1p_2\rangle.$$

Indeed, in this case Eqs. (2) reduce to

$$F(x_1,x_2)_{EPR} = 1 \times \delta(x_1-x_2),$$

$$\tilde{F}(p_1,p_2)_{EPR} = \delta(p_1+p_2) \times 1, \quad (4)$$

where the factors 1 indicate that the two-dimensional wave function takes a constant (normalized) value along the axes x_1+x_2 and p_1-p_2, respectively. On the other hand, the δ functions of Eqs. (4) indicate that the EPR two-particle system is an eigenstate of both P_1+P_2 and X_1-X_2, and is then characterized by both

$$\Delta(p_1+p_2) = 0,$$

$$\Delta(x_1-x_2) = 0, \quad (5)$$

even if both the momentum and the position of each particle are completely undefined ($\Delta p_{1,2} \approx \infty$ and $\Delta x_{1,2} \approx \infty$).

As emphasized by EPR, no physical reality seems to be associated with the momentum and the position of each particle of the entangled pair (i.e., $\Delta p_{1,2} \approx \infty$, $\Delta x_{1,2} \approx \infty$). However, the inequalities of Eqs. (3) and (5) indicate the most striking physical consequence of entanglement: despite the distance between the two particles, the measurement of momentum (position) realized on one particle immediately defines the momentum (position) of the other particle. Furthermore, the two-particle entangled system behaves as a two-dimensional wave packet defined in both the space (x_1+x_2, x_1-x_2) and the space (p_1+p_2, p_1-p_2). This last conclusion is pictorially represented by the shaded rectangles of Fig. 3.

These results are a consequence of 2D Fourier transforms; hence, there is no violation of the uncertainty principle. In fact, based on Eqs. (2) and (4), the uncertainty principle is satisfied by pairs of conjugate variables:

$$\Delta(x_1+x_2)\Delta(p_1+p_2) \geqslant \hbar,$$

$$\Delta(x_1-x_2)\Delta(p_1-p_2) \geqslant \hbar. \quad (6)$$

On the other hand, since (x_1-x_2) and (p_1+p_2) are not Fourier-conjugate variables, *their uncertainties are completely independent of each other*, and even the result $\Delta(p_1+p_2)=0$ and $\Delta(x_1-x_2)=0$, simultaneously, is acceptable. As we will clarify in the following section, this result is a distinctive property of two-particle entangled systems—i.e., is a direct consequence of the coherent superposition of two-particle amplitudes, which cannot be achieved by any system of independent quanta.

B. Systems of two independent quanta

Let us now consider an arbitrary system composed of pairs of independent quanta. From a statistical point of view, the independence between two particles is formulated as

$$\Delta(p_1 \pm p_2) = \sqrt{\Delta p_1^2 + \Delta p_2^2},$$

$$\Delta(x_1 \pm x_2) = \sqrt{\Delta x_1^2 + \Delta x_2^2}, \quad (7)$$

where Δp_j and Δx_j are the uncertainties in momentum and position associated with particle j (with $j=1,2$). The uncertainty principle prohibits the result $\Delta p_{1,2}\Delta x_{1,2}=0$; therefore, a system of independent quanta can never achieve both

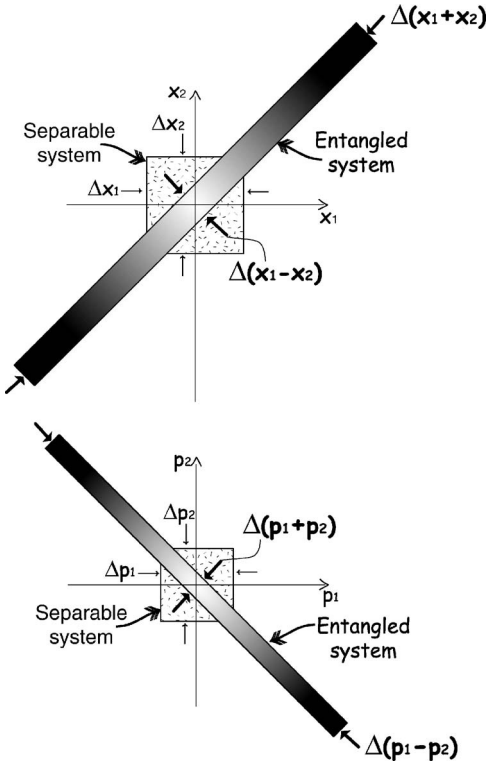

FIG. 3. Pictorial representation of the inequalities of Eqs. (3) and (8), characterizing, respectively, entangled (shaded rectangle) and separable (dotted square) systems of two quanta. The dimensions of the squares in position and momentum spaces are related to each other by the uncertainty relation $\Delta p_{1,2}=\hbar/(2\Delta x_{1,2})$, while the dimensions of the shaded rectangles are related by the uncertainty relations $\Delta(p_1+p_2)=\hbar/\Delta(x_1+x_2)$ and $\Delta(p_1-p_2)=\hbar/\Delta(x_1-x_2)$ [Eqs. (6)].

$\Delta(p_1+p_2)=0$ and $\Delta(x_1-x_2)=0$. Furthermore, for $\Delta p_1=\Delta p_2$ and $\Delta x_1=\Delta x_2$, Eqs. (7) reduce to

$$\Delta(p_1 \pm p_2) = \sqrt{2}\Delta p_1,$$

$$\Delta(x_1 \pm x_2) = \sqrt{2}\Delta x_1 \geqslant \sqrt{2}\frac{\hbar}{2\Delta p_1}. \tag{8}$$

The inequality in the last expression of Eqs. (8) is simply the uncertainty relation. Equations (8) imply that, *even if* (p_1+p_2) *and* (x_1-x_2) *are not Fourier-conjugate variables*, independent particles must satisfy the inequality

$$\Delta(p_1+p_2)\Delta(x_1-x_2) \geqslant \hbar, \tag{9}$$

due to the dependence between the uncertainties Δx_j and Δp_j $(j=1,2)$. Notice that Eq. (9) is a *consequence of the uncertainty principle* applied to each independent particle, but *does not represent an uncertainty relation* [26].

From a practical point of view, Eq. (9) indicates that, for separable systems, any attempt to reduce the uncertainty characterizing joint measurements in momentum automatically causes a loss of accuracy in the results of joint measurements performed in position (and vice versa). A pictorial representation of this result is given in Fig. 3.

C. Classical versus quantum correlation

For any separable system of pairs of quanta, each one characterized by the minimum uncertainties $\Delta p_{1,2}=\sigma_{1,2}$, and $\Delta x_{1,2}=\hbar/(2\sigma_{1,2})$, we have

$$\Delta(p_1+p_2) \geqslant \sqrt{\sigma_1^2+\sigma_2^2} > \Delta p_{1,2},$$

$$\Delta(x_1-x_2) \geqslant \frac{\hbar}{2}\sqrt{\frac{1}{\sigma_1^2}+\frac{1}{\sigma_2^2}} > \Delta x_{1,2}. \tag{10}$$

The equalities hold both for factorable pure states $(|\Psi\rangle_{1\otimes 2}=|\varphi\rangle_1|\phi\rangle_2)$ and for certain incoherent statistical mixtures of factorable states. An example is given by systems of pairs of particles having perfectly anticorrelated average momenta $[\rho_{1\otimes 2}=\Sigma_{\bar{p}_0}W(\bar{p}_0)\rho_1^{(\bar{p}_0)}\rho_2^{(-\bar{p}_0)}]$. One such system will be considered in Sec. V.

Based on Eqs. (10), *classical correlation* may exist between average momenta and/or average positions of pairs of quanta, but *the uncertainties around such average values are always independent, uncorrelated*. The reason behind this effect resides in the intrinsic independence between pairs of particles in an incoherent statistical mixture: each independent particle has to satisfy the uncertainty principle separately.

Quantum entanglement, on the contrary, involves a correlation between the uncertainties associated with each subsystem [see Eqs. (3) and (5)]. This is a result of the coherent superposition of two-particle amplitudes.

D. Summary

The minimum uncertainties in joint measurements are dictated by the nature of the subsystems on which measurements are performed (see Fig. 3).

For separable systems, the uncertainties $\Delta(p_1+p_2)$ and $\Delta(x_1-x_2)$ can never be smaller than the sum of the uncertainties associated with each independent subsystem [Eqs. (7), (8), and (10)]. In particular, Eq. (9) explicitly indicates that, for separable systems, the uncertainties $\Delta(p_1+p_2)$ and $\Delta(x_1-x_2)$ can never be independent of each other and can never be simultaneously equal to zero. Therefore, classical correlation may exist between average values of either momenta or positions of two quanta, but no correlation can ever exist between the uncertainties characterizing each particle of a separable ensemble [namely, between σ_1 and σ_2, or between $\hbar/(2\sigma_1)$ and $\hbar/(2\sigma_2)$], as indicated by Eq. (10). The physics behind these impossibilities is quite clear: each particle has its own physical reality and no action at a distance exists.

On the other hand, both the EPR state and the more general entangled state of Eq. (1) violate the inequality of Eq. (9). The uncertainties $\Delta(p_1+p_2)$ and $\Delta(x_1-x_2)$ can be indefinitely small, even zero [see Eqs. (3) and (5)]. Therefore, these systems go beyond all the above classical limitations. This is a consequence of the coherent superposition of two-particle amplitudes, which allows the uncertainties in both momentum and position to be correlated.

Entangled two-particle systems cannot be thought of as simple pairs of particles. If one insists on considering an

entangled two-particle system as composed of two independent particles, paradoxes such as EPR [8] and Popper's [9] may be inevitable. From a "local" and "realistic" physical perspective the consequences of entanglement are actually counterintuitive. However, the independence between the uncertainties $\Delta(p_1+p_2)$ and $\Delta(x_1-x_2)$, which may characterize entangled systems, is a direct consequence of 2D Fourier transforms; thus, *there is no violation of the uncertainty principle*.

Despite the difficulties in the interpretation of the concept of quantum entanglement, the "EPR inequalities" presented in this section suggest interesting practical advantages: *joint measurements realized on entangled two-particle systems allow high accuracy, beyond the classical limitations*.

III. OPERATIONAL APPROACH FOR POSITION AND MOMENTUM MEASUREMENTS OF PHOTONS

The main goal of this paper is to study the practical consequences of the EPR inequalities in the frame of ghost imaging. However, before entering in this discussion, it is necessary to define the meaning of position and momentum measurements realized on photons. In fact, the absence of a position operator for photons gives rise to several conceptual problems: (1) do the inequalities considered in Sec. II apply equally well to separable and entangled systems of photon pairs? (2) How can these uncertainties be measured in practice? (3) What do they represent? In this section, we propose an operational approach which enables us to answer these questions.

A. Extension of Fourier optics to a single photon

The momentum of the electromagnetic field is defined in classical electrodynamics as the volume integral of the energy flux density (given by the Poynting vector) divided by c^2, where c is the speed of light in vacuum. The wave vector of an electromagnetic wave points in the direction of the energy flux and its magnitude is related to the frequency of the oscillation by the relation $|\vec{k}|=\omega/c$ (in free space). Furthermore, the wave vector is related to the momentum of a photon through the well-known quantum mechanics relation $\vec{p}=\hbar\vec{k}$. Despite these standard definitions, we choose to refer to $\vec{k}$ as momentum. This choice is made to simplify the notation, but does not affect the significance of the results.

Based on classical Fourier optics [27], the transverse momentum distribution is observed in the far-field zone (or Fourier-transform plane) of an aperture. The measurement of transverse momentum is characterized by the collection of the energy propagating in a well-defined direction, but spread over a large transverse area, into one "point" of the Fourier-transform plane. In practice, the dimensions of this "point" are limited by diffraction. Transverse momentum and transverse position (i.e., transverse spatial dimension) are Fourier-conjugate variables. Hence, the limitations imposed by quantum mechanics on the accuracy of momentum and position measurements are expressed, in classical Fourier optics, by the uncertainty relation for Fourier-conjugate variables [28].

Let us now focus on the definition of position. An aperture localizes the light which passes through it and, in classical Fourier optics, is described in terms of position variables. Therefore, measurements of transverse position can be realized either in the plane of the aperture itself or in the corresponding image plane, which is defined, for instance, by the Gaussian thin-lens equation. The role of a lens in an imaging process is to collect all transverse momenta diffracted by each object point and recombine them into the corresponding image "point," as depicted in Fig. 1(a). The finite size of the imaging lens prohibits collecting all possible transverse momenta; this restriction causes the point-to-point relationship between the object and the image plane to become a point-to-"spot" relationship. The dimensions of the "spot" define the spatial resolution of the image and represent the uncertainty in the position measurement: $\Delta(\vec{\rho}_{im}-\vec{\rho}_{obj})$. The resolution of the image is strictly related to the amount of transverse momenta collected by the lens ($\Delta\vec{\kappa}_{coll}$), which is defined by the numerical aperture X_{NA} of the imaging lens.

From an operational point of view, the Fourier-optics definitions of both position and momentum measurements can be applied to a single photon: an aperture and its corresponding image plane measure the position of any transmitted photon, while its transverse momentum can be measured in the far-field zone (or Fourier-transform plane) of the aperture. This is in line with the argument adopted by Feynmann [29].

Care must be taken not to confuse a projection with an image: projection is the shadow of an object [see Fig. 1(b)]. Also notice that the observation of a projection corresponds to the measurement of a finite amount of momenta and contains partial information about position, as well.

The above operational definitions represent a tool to identify the variables measured in an arbitrary optical setup and to interpret the results of any measurement realized on photons. In the next sections, we will extend the operational approach to systems of photon pairs. In particular, we will consider the optical setup for implementing both momentum-momentum and position-position EPR correlation measurements; this will allow us to evaluate the uncertainties in the sum of transverse momenta $[\Delta(\vec{\kappa}_1+\vec{\kappa}_2)]$ and in the difference of transverse positions $[\Delta(\vec{\rho}_1-\vec{\rho}_2)]$ of photon pairs. The practical implications of the inequalities discussed in Sec. II, in the frame of ghost imaging, will then become clear.

B. Systems of photon pairs

The properties of a system of photon pairs can be studied by counting coincidences between two spatially separated single-photon detectors (D_1 and D_2). The rate of coincidence counts is evaluated by using Glauber's formula for the second-order correlation function [30]

$$G^{(2)}(\vec{r}_1,\vec{r}_2,t_1,t_2)=\mathrm{tr}[E_1^{(-)}(\vec{r}_1,t_1)E_2^{(-)}(\vec{r}_2,t_2)\times E_2^{(+)}(\vec{r}_2,t_2)E_1^{(+)}(\vec{r}_1,t_1)\rho_{12}], \quad (11)$$

which represents the joint probability of detecting a photon in the space-time location $(\vec{r}_1,t_1)$ and a photon in the space-time location $(\vec{r}_2,t_2)$, for any system described by the density

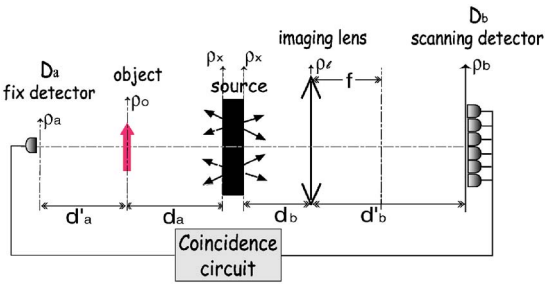

FIG. 4. (Color online) Schematic of the setup for implementing EPR correlation measurements on optical sources. The source emits pairs of photons in all possible directions, but always with opposite momenta. The system of photons can either be entangled or separable. For practical implementations, one should consider the folded version of this setup.

matrix ρ_{12}. In Eq. (11), $E_1^{(\pm)}(\vec{r}_1,t_1)$ and $E_2^{(\pm)}(\vec{r}_2,t_2)$ are the quantized field operators at detectors D_1 and D_2, respectively. The fields at the detectors can be expressed in terms of the field on the output plane of the source by using the Green's functions of Gaussian optics, also called optical transfer functions [31,32]. In the *paraxial approximation* we have

$$E_j^{(+)}(\vec{r}_j,t_j) = C\int d\vec{\kappa}\int d\omega a_{\vec{k}} e^{-i\omega(\vec{k})t_j} g_j(\vec{\kappa},\omega;\vec{\rho}_j,z_j), \quad (12)$$

where $\vec{r}_j=(\vec{\rho}_j,z_j)$ defines the position of detector j with respect to the output plane of the source, t_j is the time at which the jth detector clicks, C is a normalization constant, $g_j(\vec{\kappa},\omega,\vec{\rho}_j,z_j)$ is the optical transfer function describing arm j of the setup, and $a_{\vec{k}}$ is the annihilation operator for a photon with momentum $\vec{k}=(\vec{\kappa}_j,k_z\approx|\vec{k}|)$, for $j=1,2$.

In the quantized field of Eq. (12), the description of the optical setup is always included in the g_j functions given by classical Gaussian optics; on the other hand, the quantized field operator $a_{\vec{k}}$ describes the annihilation of a photon with momentum $\vec{k}$. Therefore, by choosing the optical setup (i.e., the g_j functions) based on the operational approach developed in Sec. III A, one may measure both momentum and position variables also on systems of photon pairs. From this perspective, it becomes clear that the second-order correlation function $G^{(2)}(\vec{r}_1,\vec{r}_2,t_1,t_2)$ may represent *the probability distribution of both position-position and momentum-momentum variables*, depending on the optical setup. This probability distribution can then be used to evaluate the uncertainties $\Delta(\vec{\kappa}_1+\vec{\kappa}_2)$ and $\Delta(\vec{\rho}_1-\vec{\rho}_2)$.

C. Setup for implementing EPR experiments on systems of photons

Using the above definitions, we can identify the setups for implementing both position-position and momentum-momentum EPR correlation measurements on systems of photons. The basic setup is drawn in Fig. 4: in arm a photons propagate freely over the distance d_a from the output plane of the source to the object, and a point like detector D_a is placed at a distance d_a' behind it. In arm b photons propagate freely over the distance d_b from the output plane of the source to the imaging lens (of focal length f), and a pointlike detector D_b is placed at a distance d_b' behind it. In the paraxial approximation, the fields at detectors D_a and D_b are given by Eq. (12), with $z_j=d_j+d_j'$, with $j=a$, and b, respectively. In order to implement the two EPR measurements we need detector D_a to measure either momentum or position variables; we will then consider two special cases.

To measure the momentum of photons propagating in arm a of the setup, we need to place the pointlike detector D_a in the far field of the object $[\omega D^2/(cd_a')\ll 1]$ or, equivalently, in the focal plane of a converging lens ($d_a'=f_{coll}$). As we prove in the Appendix, in this case, the field at detector D_a is given by

$$E_a^{(+)}(\vec{\rho}_a,z_a=d_a+f_{coll};t_a)_{(MOM)} = C\frac{-i\omega}{2\pi c f_{coll}}\int d\omega e^{-i\omega(t_a-(z_a/c))}G(|\vec{\rho}_a|)_{[\omega/(cf_{coll})]} \times\int d\vec{\kappa}G(|\vec{\kappa}|)_{[-cd_a/\omega]}\tilde{T}\left(\vec{\kappa}-\frac{\omega}{cf_{coll}}\vec{\rho}_a\right)a_{\vec{k}}, \quad (13)$$

where $\tilde{T}$ is the Fourier transform of the object transfer function $t(\vec{\rho}_o)$ and $G(|\alpha|)_{[\beta]}=e^{i\beta/2|\alpha|^2}$ is a Gaussian function of $|\alpha|$, whose imaginary variance is related to the parameter β (see the Appendix). Based on Eq. (13), detector D_a collects in the location $\vec{\rho}_a$ all diffracted photons having transverse momentum $\vec{\kappa}=\omega/(cf_{coll})\vec{\rho}_a$.

Replacing the pointlike detector D_a by a "bucket detector," we can measure all photons which pass through the object independently on their momenta. As we discuss in the Appendix, detector D_a has now a wide sensitive area and is placed in the focal plane of a short focal length converging lens (i.e., $d_a'=f_{coll}$); the field in one point of detector D_a is again given by

$$E_a^{(+)}(\vec{\rho}_a,z_a=d_a+f_{coll};t_a)_{(POS)} = C\frac{-i\omega}{2\pi c f_{coll}}\int d\omega e^{-i\omega(t_a-(z_a/c))}G(|\vec{\rho}_a|)_{[\omega/(cf_{coll})]} \times\int d\vec{\kappa}G(|\vec{\kappa}|)_{[-cd_a/\omega]}\tilde{T}\left(\vec{\kappa}-\frac{\omega}{cf_{coll}}\vec{\rho}_a\right)a_{\vec{k}}. \quad (14)$$

Following standard Glauber's theory, the integration over the area of the detector will be done after evaluating the second-order correlation function $G^{(2)}(\vec{\rho}_a,\vec{\rho}_b)$. In this case, detector D_a measures the position of photons within the dimension of the object (A_{obj}), and no information is obtained about their momenta.

Evaluating the optical transfer function g_b describing arm b of the setup of Fig. 4, we obtain, for the field at detector D_b (see the Appendix),

$$E_b^{(+)}(\vec{\rho}_b,z_b=d_b+d_b';t_b) = C\frac{-i\omega}{2\pi c d_b'}\int d\omega e^{-i\omega(t_b-(z_b/c))}G(|\vec{\rho}_b|)_{[\omega/(cd_b')]} \times\int d\vec{\kappa}G(|\vec{\kappa}|)_{[-cd_b/\omega]}\int_{A_{lens}} d\vec{\rho}_l e^{i\{\vec{\kappa}-[\omega/(cd_b')]\vec{\rho}_b\cdot\vec{\rho}_l}$$

$$\times G(|\vec{\rho}_l|)_{[(\omega/c)(1/d_b'-1/f)]}a_{\vec{k}}, \quad (15)$$

where $\vec{\rho}_l$ is a two-dimensional vector defined on the transverse plane of the lens (whose transverse area is A_{lens}).

IV. GHOST IMAGING WITH ENTANGLED PHOTON PAIRS

In this section we will extend the results found in Sec. II A to entangled two-photon systems. The definitions of position and momentum measurements given in the previous section will lead us to interpret the EPR inequalities of Sec. II in terms of the spatial resolution and the visibility of ghost imaging effects.

A. SPDC: A source of entangled photon pairs

Our goal is to evaluate the second-order correlation function for the setup of Fig. 4, when the source emits entangled two photon system. To this end we consider the two-photon system produced by degenerate and approximately collinear type-II SPDC [32–34]:

$$|\Psi_{SPDC}\rangle = A \int d\nu e^{iLD\nu/2}\mathrm{sinc}(LD\nu/2) \int d\vec{\kappa}_i \times \int d\vec{\kappa}_s h_{\mathrm{tr}}(|\vec{\kappa}_i + \vec{\kappa}_s|)a_i^\dagger(\vec{k}_i)a_s^\dagger(\vec{k}_s)|0\rangle, \quad (16)$$

where L is the length of the SPDC crystal, ν is the frequency detuning with respect to the central frequencies $\Omega_s=\Omega_i=\Omega_p/2$ of signal (s) and idler (i), $D=1/u_s-1/u_i$, with u_j group velocity at the central frequency Ω_j (for $j=i,s$), $\vec{\kappa}_j$ is the transverse wave vector of the photon, and $a_j^\dagger(\vec{k}_j)$ is the creation operators for a photon in the mode defined by the momentum $\vec{k}_j$, for $j=i,s$. The function h_{tr} is the Fourier transform of the pump transverse profile; for instance, if the pump beam has a Gaussian transverse profile $[f(\vec{\rho})=e^{-\sigma_p^2|\vec{\rho}|^2/2}]$, then $h_{\mathrm{tr}}(|\vec{\kappa}_i+\vec{\kappa}_s|)=e^{-|\vec{\kappa}_i+\vec{\kappa}_s|^2/(2\sigma_p^2)}$. Notice that the "thin-crystal approximation" [$L\tan(\theta)\ll\sigma_p^{-1}$, where θ is the scattering angle of the signal-idler radiation inside the crystal] has been inserted in the argument of the frequency integral in Eq. (16). In this approximation, the dependence of both the sinc function and the phase factor on the transverse momentum can be neglected [32,34]. In the following discussion, we will assume that the object itself selects only the idler photons which satisfy the thin-crystal approximation. For instance, if θ' is the maximum scattering angle for which the condition $L\tan(\theta')<\sigma_p^{-1}$ is satisfied, we will only consider objects whose transverse dimension D_{obj} is such that $D_{obj}\leqslant d_a\tan(\theta')$.

Equation (16) indicates that the SPDC signal-idler pairs are generated in such a way that the energy and the momentum of neither photon are determined. However, if one photon is detected with a certain energy and momentum, the energy and momentum of its twin are immediately known with a very small uncertainty (given by the variance of the sinc and h_{tr} function, respectively). The pair can only be described as an entangled two-photon system [35].

It is interesting to realize that, in the approximation we are considering, the SPDC state of Eq. (16) is characterized by pure anticorrelation in transverse momentum; i.e., it falls in the class of entangled states described by Eq. (1), with $\tilde{A}(\vec{\kappa}_i+\vec{\kappa}_s)=e^{-|\vec{\kappa}_i+\vec{\kappa}_s|^2/(2\sigma_p^2)}$ and $\tilde{C}(\vec{\kappa}_i-\vec{\kappa}_s)=$const. Following this analogy, we expect the uncertainties in the sum of the momenta and in the difference of the positions of the SPDC two-photon system to satisfy Eqs. (3).

For entangled two-photon systems, the second-order correlation function of Eq. (11) simplifies to

$$G^{(2)}\left(\vec{\rho}_1,\vec{\rho}_2,T_1=t_1-\frac{z_1}{c},T_2=t_2-\frac{z_2}{c}\right) = |\langle 0|E_1^{(+)}(\vec{\rho}_1,T_1)E_2^{(+)}(\vec{\rho}_2,T_2)|\Psi_{SPDC}\rangle|^2 = |\Psi_{12}(\vec{\rho}_1,\vec{\rho}_2,T_1,T_2)|^2, \quad (17)$$

where $\Psi_{12}(\vec{\rho}_1,\vec{\rho}_2,T_1,T_2)$ is the so-called "biphoton amplitude" [33,36]. The existence of such a biphoton amplitude is a direct consequence of the entangled nature of the signal-idler pairs emitted by SPDC [12,36]. Based on the result of Eqs. (16) and (17), the double-arrowed straight lines of Figs. 2 and 4 assume a very particular meaning: each straight line is a two-photon probability amplitude; all straight lines exist simultaneously and are coherently superposed. In principle, all straight lines (or two-photon probability amplitudes) are associated with just one signal-idler pair.

B. Quantum ghost image and interference: EPR experiments for entangled photon pairs

By inserting in Eq. (17) the expressions of the fields at the detectors of Eqs. (13) and (15), we obtain the biphoton amplitude describing the EPR setup for measuring transverse momentum on the idler photons:

$$\begin{aligned}\Psi_{12}(\vec{\rho}_1,T_1,\vec{\rho}_2,T_2)_{(MOM)} &= CG(|\vec{\rho}_1|)_{[\Omega_p/(2cf_{coll})]}G(|\vec{\rho}_2|)_{[\Omega_p/(2cd_b')]}e^{-i\Omega_pT_+}e^{-i\Omega_dT_-} \\ &\times \int d\nu e^{i\nu((LD/2)-T_-)}\mathrm{sinc}\left(\frac{LD\nu}{2}\right)\int d\vec{\kappa}_i \\ &\times \int d\vec{\kappa}_s h_{\mathrm{tr}}(\vec{\kappa}_i+\vec{\kappa}_s)G(|\vec{\kappa}_i|)_{[-2cd_a/\Omega_p]}G(|\vec{\kappa}_s|)_{[-2cd_b/\Omega_p]} \\ &\times \tilde{T}\left(\vec{\kappa}_i-\frac{\Omega_p}{2cf_{coll}}\vec{\rho}_1\right)\int_{A_{lens}} d\vec{\rho}_l G(|\vec{\rho}_l|)_{\{[\Omega_p/(2c)](1/d_b'-1/f)\}} \\ &\times e^{i\{\vec{\kappa}_s-[\Omega_p/(2cd_b')]\vec{\rho}_2\}\vec{\rho}_l}, \end{aligned} \quad (18)$$

where $T_+=(T_1+T_2)/2$ and $T_-=T_1-T_2$, $\Omega_p=\Omega_s+\Omega_i$, and $\Omega_d=(\Omega_s-\Omega_i)/2$ (which in the degenerate case is equal to zero). All terms in ν coming from the G functions (second- and higher-order terms in ν/Ω_p) have been neglected; this allows the factorization of the biphoton amplitude into a temporal and a (transverse) spatial part, as shown in Eq. (18). The integration over the frequency detuning ν gives the Fourier transform of the sinc function: a square function $\Pi(T_-+LD)$ extending from 0 to DL [33,36]. The temporal part of the biphoton is then given by the product of a function

$v(T_+)=e^{-i\Omega_p T_+}$ times a function $u(T_-)=e^{-i\Omega_d T}\Pi(T_-+LD)$. This is the time-frequency counterpart of the result obtained in Sec. II A for momentum-position variables [Eq. (2)]. This term indicates that the correlation in transverse momentum of the SPDC biphoton can only be exploited by performing coincidence measurements within the coherence time of the biphoton [defined by $\Pi(T_-+LD)$] [32].

Let us now focus on the spatial (transverse) part of the biphoton amplitude. Inspection of Eq. (18) suggests that a simple and interesting result appears when detector D_b is placed in the focal plane of the imaging lens ($d_b'=f$). In this case, the integration over the transverse area of the imaging lens gives a δ function in $[\vec{\kappa}_s-\vec{\rho}_2\Omega_p/(2cf)]$. This result indicates that only one transverse momentum of the signal photons reaches the location $\vec{\rho}_2$ of the pointlike detector D_b. After using this δ function to perform the integration in $\vec{\kappa}_s$, we get

$$G^{(2)}(\vec{\rho}_1,\vec{\rho}_2)_{(MOM)} \propto \left| \int d\vec{\kappa}_i G(|\vec{\kappa}_i|)_{[-2cd_a/\Omega_p]} \times \tilde{T}\left(\vec{\kappa}_i - \frac{\Omega_p}{2cf_{coll}}\vec{\rho}_1\right) \times h_{\mathrm{tr}}\left(\left|\vec{\kappa}_i + \frac{\Omega_p}{2cf}\vec{\rho}_2\right|\right)\right|^2. \quad (19)$$

For any $\vec{\rho}_2$ satisfying the condition $\vec{\kappa}_s=\vec{\rho}_2\Omega_p/(2cf)$ and for any fixed value of $\vec{\rho}_1$ (in the focal plane of the collection lens), the biphoton amplitude is the convolution of the Fourier transform ($\tilde{T}$) of the object transfer function with the angular spectrum of the SPDC radiation (h_{tr}) and the envelope of the radiation on the aperture plane (G). For a perfect plane-wave pump beam [i.e., for $h_{\mathrm{tr}}=\delta(\vec{\kappa}_s+\vec{\kappa}_i)$], *the biphoton amplitude is simply the Fourier transform of the object* $\{G^{(2)}(\vec{\rho}_1,\vec{\rho}_2)_{(MOM)}\propto|\tilde{T}[\vec{\rho}_2\Omega_p/(2cf)+\vec{\rho}_1\Omega_p/(2cf_{coll})]|^2\}$; in other words, the ghost interference-diffraction pattern of the aperture inserted in the idler arm is reproduced by the coincidence counts on the signal side and is characterized by 100% visibility. This is the result of perfect anticorrelation in transverse momentum $[\Delta(\vec{\kappa}_s+\vec{\kappa}_i)=0]$.

Based on the result of Eq. (19), the visibility of the ghost interference pattern is affected by the imperfect momentum-momentum correlation, described by the nonzero width of h_{tr}. Therefore, the uncertainty in $\vec{\kappa}_i+\vec{\kappa}_s$ is simply the variance of the correlation function $h_{\mathrm{tr}}(\vec{\kappa}_i+\vec{\kappa}_s)$; this demonstrates that the SPDC signal-idler pairs satisfy the inequality

$$\Delta(\vec{\kappa}_i+\vec{\kappa}_s)=\sigma_p \ll \Delta\vec{\kappa}_{i,s}, \quad (20)$$

where the uncertainty $\Delta\vec{\kappa}_i$ is the variance of the single counts distribution on the idler side $[I(\vec{\rho}_1)=\mathrm{tr}_i(E_1^{(-)}E_1^{(+)}\rho_i)]$; the same definition applies to $\Delta\vec{\kappa}_s$. Notice that, for the result of Eq. (19) to be observable, the intensity distribution at both detectors' planes needs to be fairly constant; hence, *pure second-order* (or, equivalently, ghost) effects are generally accompained by large values of the uncertainties $\Delta\vec{\kappa}_{i,s}$.

The results of Eqs. (19) and (20) may be easily interpreted in EPR terms: the momenta of both photons are completely uncertain; however, when the momentum of the idler is measured in the far field of an aperture, the momentum of the corresponding signal acquires a "well-defined" value (within the uncertainty due to the lack of perfect correlation), such that the Fourier transform of the aperture is reproduced on the signal side. Notice that the well-defined momentum of the signal can only be measured in momentum space, here represented by the focal plane of the imaging lens ($d_b'=f$).

This is only half of the EPR thought experiment. Let us now consider its second half: by employing a bucket detector in arm a of the setup, the position of the idler photons can be measured within the uncertainty defined by the dimension of the object. The biphoton amplitude can now be evaluated by substituting into Eq. (17) the expressions of the fields at the detectors given in Eqs. (14) and (15), respectively. Neglecting the temporal part of the biphoton amplitude, we obtain, for its transverse spatial part,

$$\Psi_{12}(\vec{\rho}_1,\vec{\rho}_2)_{(POS)} \propto \int d\vec{\rho}_o t(\vec{\rho}_o) e^{-i(\Omega_p/2cf_{coll})\vec{\rho}_1\cdot\vec{\rho}_o} \int d\vec{\kappa}_+ h_{\mathrm{tr}}(\vec{\kappa}_+) G(|\vec{\kappa}_+|)_{\{(-(c/2\Omega_p)\{d_a+d_b+[(1/(1/d_b'-1/f)]\})} \exp\left[i\frac{\vec{\kappa}_+}{2}\cdot\left(\vec{\rho}_o+\frac{1}{1-\frac{d_b'}{f}}\vec{\rho}_2\right)\right] \times \int d\vec{\kappa}_- G(|\vec{\kappa}_-|)_{\{(-(2c/\Omega_p)\{d_a+d_b+[(1/(1/d_b'-1/f)]\}} \exp\left[i\vec{\kappa}_-\cdot\left(\vec{\rho}_o-\frac{1}{1-\frac{d_b'}{f}}\vec{\rho}_2\right)\right] \exp\left[-i\frac{c}{\Omega_p}\left(d_a-d_b-\frac{1}{\frac{1}{d_b'}-\frac{1}{f}}\right)\vec{\kappa}_+\cdot\vec{\kappa}_-\right], \quad (21)$$

where we have assumed the lens to have infinite transverse dimension and we have introduced the new variables $\vec{\kappa}_+=\vec{\kappa}_i+\vec{\kappa}_s$ and $\vec{\kappa}_-=(\vec{\kappa}_i-\vec{\kappa}_s)/2$. A close inspection of the argument of the G functions indicates that, for a given value of both $s_o=d_a+d_b$ and f, the two-photon Gaussian thin-lens equation $1/s_o+1/s_i=1/f$ defines a unique plane on the signal side ($d_b'=s_i$) where a magnified image of the object can be observed ($m=-s_i/s_o$) [2]. Therefore, by imposing the condi-

tion $1/s_o+1/s_i=1/f$ to the biphoton amplitude of Eq. (21) and performing the integration in both $\vec{\kappa}_+$ and $\vec{\kappa}_-$, we find

$$\Psi_{12}(\vec{\rho}_1,\vec{\rho}_2)_{(POS)} \propto \int d\vec{\rho}_o t(\vec{\rho}_o) G(|\vec{\rho}_o|)_{[\Omega_p/2cd_a]} \times h_{\mathrm{tr}}\left[\frac{\Omega_p}{2cd_a}\left(\frac{\vec{\rho}_2}{m}-\vec{\rho}_o\right)\right] e^{-i(\Omega_p/2cf_{coll})\vec{\rho}_1\cdot\vec{\rho}_o}. \quad (22)$$

Now, by integrating the modulus square of the above biphoton amplitude over the whole sensitive area of the bucket detector D_a, we obtain the second-order correlation function describing the EPR position-position measurement:

$$G^{(2)}(A_{obj},\vec{\rho}_2)_{(POS)} \propto \int_{A_{obj}} d\vec{\rho}_1 |t(\vec{\rho}_1)|^2 \left| h_{\mathrm{tr}}\left[\frac{\Omega_p}{2cd_a}\left(\frac{\vec{\rho}_2}{m}-\vec{\rho}_1\right)\right]\right|^2. \quad (23)$$

In other words, the second-order correlation function is now given by the convolution of the squared object transfer function ($|t|^2$) with the modulus square of the spatial correlation function of the SPDC radiation ($|h_{\mathrm{tr}}|^2$). Notice that, since we assumed the lens to have infinite transverse dimension, the spatial correlation function $|h_{\mathrm{tr}}|^2$ plays the role of a two-photon point-spread function. It is easy to prove that, when the finite dimension of the lens is taken into account, the function $P[\Omega_p/(2c)X_{NA}(\vec{\rho}_2/m-\vec{\rho}_o)]$ (with $X_{NA}=R_{lens}/s_o$) appears in the argument of the integral as well. On the other hand, for a plane-wave pump and an infinite lens, we would have $G^{(2)}(A_{obj},\vec{\rho}_2)_{(POS)} \propto |t(\vec{\rho}_2/m)|^2$, which is the stigmatic image of the object magnified by a factor of $m=-s_i/s_o$. This result indicates a perfect point-to-point correspondence between the object and the two-photon ghost image plane $[\Delta(\vec{\rho}_s-\vec{\rho}_i)=0]$.

The meaning of this result in EPR terms is clear: the position of both photons is unknown; however, when the position of the idler is measured on the object plane, the position of the corresponding signal acquires a well-defined value and a point-to-point correspondence arises between the object and the ghost image planes. The well-defined position of the signal can only be measured in position space, whose existence, on the signal side, is guaranteed by the two-photon Gaussian thin-lens equation.

The imperfect point-to-point correspondence between object and ghost image planes is quantified by the uncertainty

$$\Delta(\vec{\rho}_s-\vec{\rho}_i) \lesssim \sqrt{\frac{(d_a\lambda_p\sigma_p)^2}{2\pi^2}+\left(1.22\frac{\lambda_p}{X_{NA}}\right)^2} \ll \Delta\vec{\rho}_{s,i}, \quad (24)$$

where the first term in the argument of the square root accounts for the finite size of the pump beam (i.e., for imperfect momentum-momentum two-photon correlation) and the second one is the diffraction limit, due to the finite size of the imaging lens. The uncertainty $\Delta(\vec{\rho}_i)$ is defined by the dimension of the object and $\Delta(\vec{\rho}_s)$ can be estimated from the intensity distribution of the signal photons on the scanning plane.

The result of Eq. (24) is in agreement with the second EPR inequality of Eqs. (3), but the quantitative values of the uncertainties $\Delta(\vec{\rho}_s-\vec{\rho}_i)$ are different. In fact, even though we are dealing with an entangled state purely anticorrelated in momentum [notice the analogy between Eqs. (1) and (16)], the biphoton amplitude associated with the ghost imaging setup does not factor into a function of $\vec{\rho}_o+\vec{\rho}_2/m$ times a function of $\vec{\rho}_o-\vec{\rho}_2/m$ [compare Eq. (2) with both Eqs. (21) and (22)]. This is not in contradiction with the results of Sec. II A; it simply indicates that *the ghost imaging setup* implies coupling of both the $\vec{\kappa}_\pm$ and the $\vec{\rho}_\pm$ variables. The practical consequence of this effect is that quantum ghost images are affected by Rayleigh diffraction and their resolution depends on the pump size, as indicated by Eq. (24). This result is quite interesting, since it explicitly demonstrates that the intrinsic properties of an entangled two-photon system are very sensitive to the experimental setup in which the system propagates.

One may wonder if entangled two-photon states can ever overcome the Rayleigh diffraction limit and give rise to superresolved images. The answer is positive, if an adequate optical setup is employed. In fact, the basic idea of quantum lithography [6,7] is to overcome the Rayleigh diffraction limit by exploiting the N-photon diffraction of an entangled N-photon system.

An experimental verification of the idea presented here has been recently realized by our group [11]. The results agree with the theoretical predictions developed in this section: the coherent superposition of two-photon amplitudes characterizing the SPDC radiation allows obtaining ghost imaging effects characterized by almost 100% visibility and high resolution, as quantitatively expressed by Eqs. (20) and (24). The high contrast and accuracy achieved by entangled two-photon systems can never be obtained "classically" [25].

C. Popper's thought experiment

Another interesting consequence of entanglement was formulated by Popper in the form of a thought experiment [9]. The idea is very similar to EPR's: the quantum correlation between entangled two-particles implies the possibility of knowing, with high precision, both the position and the momentum of one subsystem. Therefore, Popper believed that entangled systems may violate the uncertainty principle.

The first experimental realization of Popper's thought experiment has been performed by our group some years ago [10], by employing an SPDC two-photon source. Surprisingly, the experimental observations agreed with Popper's prediction: the existence of a highly resolved ghost image implies the possibility of localizing a photon without disturbing its momentum. Here, we will analyze Popper's experiment from the theoretical point of view and we will show

that, despite the correctness of Popper's predictions, no violation of the uncertainty principle can be associated with the experimental results, in line with the conclusion reached in [10].

As we have shown in the previous section, the entangled nature of the SPDC radiation allows one to reproduce a ghost mage of an object by counting coincidences between a fixed bucket detector D_a and a scanning pointlike detector D_b; the ghost image plane is identified by a two-photon thin-lens equation. Popper's experiment can be realized by comparing the patterns obtained at the *far-field distance* z behind the ghost image plane, in two different situations: (1) a real aperture, whose dimensions are identical to the dimension of the image, is inserted in the ghost image plane, and (2) no real aperture is inserted in the ghost image plane. For simplicity, we consider the case in which $|m|=1$. Therefore, Popper's experiment can be realized in the setup drawn in Fig. 4; we only need to take the object to be a single slit of dimension D, the longitudinal distances to give $d_a+d_b=s_o=s_i=2f$ and $d_b'=s_i+z$. Notice that, since Popper's thought experiment is based on the idea of measuring the *momentum* of photons propagating in arm b of the setup, the distance z needs to satisfy the far-field condition $D^2\omega/(cz)\ll 1$.

Let us start by considering the case in which a real single slit of dimension D is inserted in both the object and the ghost image plane. By considering the SPDC state given by Eq. (16), the field at detector D_a given by Eq. (14), and slightly modifying the field at detector D_b [Eq. (15)] to take into account the presence of a real slit in $s_i=2f$, we find

$$G^{(2)}(D,x_2) \propto \left| \mathrm{sinc}\left(\frac{\Omega_p}{2c}\frac{D}{2}\frac{x_2}{z} \right) \right|^2, \tag{25}$$

which is simply the modulus square of the Fourier transform of the object. Notice that the second-order correlation function of Eq. (25) is the perfect copy of the (first-order) diffraction pattern. This is in line with Popper's original idea: the goal of this measurement is to evaluate the uncertainty Δk_{x_s}, given $\Delta x_s=D/2$. Based on Eq. (25) we have $\Delta k_{x_s}=2/D$; therefore, in agreement with the uncertainty principle, $\Delta k_{x_s}\Delta x_s=1$ [28].

Now we remove the single slit from the ghost image plane. The second-order correlation function can then be evaluated using Eqs. (16), (14), and (15) just taking $d_b'=2f+z$. In the plane-wave approximation for the pump beam, we find

$$G^{(2)}(D,x_2) \propto \left| G(|x_2|)_{\{(\Omega_p/2cz)[1/(1+z/f)]\}} \otimes t\left(\frac{x_2}{1+z/f} \right) \right|^2 \approx \left| t\left(\frac{x_2}{1+z/f} \right) \right|^2, \tag{26}$$

which is the modulus square of the transfer function of the object, magnified by a factor $1+z/f$; this pattern represents the geometrical projection of the image. The result in the first line of Eq. (26) represents the convolution of the ghost image of the object with a Fresnel weighting factor. Hence, Eq. (26) indicates that the pattern obtained from the coincidence counts is an *out-of-focus image of the object*. Due to the absence of a real object in the signal arm, the intensity distribution in arm b does not contain first-order patterns anymore. Therefore, in this case, the second-order correlation function reproduces a pure second-order effect.

The pattern described by Eq. (26) can be much narrower than the one described by Eq. (25). For instance, in the experimental setup of [10] ($z=f=500$ mm, $\lambda_s=2\lambda_p=702$ nm, $D=0.16$ mm), the width of the diffraction pattern of Eq. (25) is $\Delta x_2^{[slit]}\approx\lambda_s f/D=2.2$ mm, while the width of the out-of-focus image described by Eq. (26) is $\Delta x_2^{[noslit]}\approx\sqrt{D^2+\lambda_s f/\pi}=0.37$ mm. Hence, in agreement with Popper's theoretical prediction,

$$\Delta x_2^{[noslit]} \ll \Delta x_2^{[slit]}. \tag{27}$$

Notice, however, that the variance $\Delta x_2^{[noslit]}$ of the probability distribution of Eq. (26) does not represent the uncertainty in the momentum of the signal photons (Δk_{x_s}). Hence, the fact that the pattern of Eq. (26) is narrower than the one described by Eq. (25) [as reported in Eq. (27)] does not represent a violation of the uncertainty relation $\Delta k_{x_s}\Delta x_s\geqslant 1$. The apparent inconsistency between entanglement and the uncertainty principle discussed by Popper derives from an improper interpretation of the predicted results: joint measurements should not be used to estimate the uncertainty in momentum of a single particle or photon.

In this respect, it is also worth emphasizing that, since Eq. (26) describes an out-of-focus image rather than the Fourier transform of the object, the variance of this pattern is much closer to the uncertainty $\Delta(x_s-x_i)$ than to the uncertainty $\Delta(k_{x_s}+k_{x_i})$. In fact, taking into account the finite size of both pump beam and imaging lens, we can estimate

$$\Delta(x_s-x_i)^2 \approx \Delta(x_s-x_i)_{IM}^2 + z\left(1+\frac{z}{f}\right)\frac{\lambda_s}{2\pi}, \tag{28}$$

which is the sum of the resolution characterizing the quantum ghost image [Eq. (24)] plus a term that accounts for the blurring of the out of focus quantum ghost image.

D. Remarks

The uncertainties $\Delta(\vec{\kappa}_1+\vec{\kappa}_2)$ and $\Delta(\vec{\rho}_1-\vec{\rho}_2)$ involved in the EPR inequalities are related, respectively, to the visibility of quantum ghost interference and to the resolution of the quantum ghost image.

Based on the results of Eqs. (18) and (22), the biphoton amplitude contains the whole ghost interference-diffraction pattern, in one case, and the point-to-point correspondence between the object and the ghost image planes, in the other. This explicitly indicates that quantum ghost imaging effects are the result of the coherent superposition of two-photon probability amplitudes. Therefore, for an entangled source, all the straight lines drawn in both Figs. 2 and 4 should be thought as coexisting and coherently superposed two-photon amplitudes associated with one signal-idler pair: in principle, one SPDC pair gives rise to the quantum ghost diffraction pattern in the focal plane of the imaging lens and to the point-to-point correspondence between the object and ghost image planes. The coherent superposition of the two-photon

amplitudes is responsible for the high visibility and high resolution characterizing quantum ghost imaging patterns [as quantified in Eqs. (20) and (24)].

From the point of view of practical applications, the results presented in this section are quite interesting: the entangled nature of the SPDC signal-idler pairs allows an accurate reproduction of nonlocal or ghost imaging patterns. The results obtained for the second-order correlation function indicate that the visibility can be, in principle, 100%. Furthermore, pump sizes of the order of a few millimeters give rise to such a strong momentum-momentum correlation that the resolution of quantum ghost images is basically only limited by diffraction effects caused by the finite imaging lens. We can then conclude that entangled two-photon systems offer the unique possibility of performing nonlocal positioning measurements, with high accuracy, even beyond the classical limit.

To clarify the concept of classical limit in the frame of coincidence measurements, we will consider two different simulations of the quantum ghost image and interference. In Sec. V, we analyze the results of ghost imaging experiments realized with *a source of pairs of photons characterized by classical statistical correlation in momentum*, and in Sec. VI, we consider *a chaotic thermal source*.

V. GHOST IMAGING WITH SEPARABLE SYSTEMS OF PHOTONS CLASSICALLY CORRELATED IN MOMENTUM

A separable system may be described quantum mechanically by an incoherent statistical mixtures of the kind: $\rho = \int d\bar{\xi}_0 p(\bar{\xi}_0) |\Psi^{(\bar{\xi}_0)}\rangle\langle\Psi^{(\bar{\xi}_0)}|$, where $\bar{\xi}_0$ is a generic variable, $p(\bar{\xi}_0)$ is a (positive) probability distribution, and

$$|\Psi^{(\bar{\xi}_0)}\rangle_{1\otimes 2} = |\varphi^{(\bar{\xi}_0)}\rangle_1 \otimes |\phi^{(\bar{\xi}_0)}\rangle_2 \tag{29}$$

is a factorable pure state. The expression "incoherent" is used to emphasize that no phase information is retained in the summation.

Here, we are interested in separable systems of photons simulating the SPDC photon pairs. To this end, we take the variable $\bar{\xi}_0$ to represent transverse momentum ($\bar{\xi}_0 = \vec{\bar{\kappa}}_0$) and the pure states $|\varphi^{(\bar{\xi}_0)}\rangle_1$ and $|\phi^{(\bar{\xi}_0)}\rangle_2$ to be single-photon pure states characterized by anticorrelation in transverse momentum:

$$|\varphi^{(\bar{\kappa}_0)}\rangle_1 = C_1 \int d\vec{\kappa} f_1(\vec{\kappa} - \vec{\bar{\kappa}}_0) |\vec{\kappa}\rangle_1,$$

$$|\phi^{(-\bar{\kappa}_0)}\rangle_2 = C_2 \int d\vec{\kappa} f_2(\vec{\kappa} + \vec{\bar{\kappa}}_0) |\vec{\kappa}\rangle_2, \tag{30}$$

where f_j (for $j=1,2$) are real functions. Hence, the density matrix for an ensemble of photons manifesting classical anticorrelation in momentum is given by

$$\rho_{1\otimes 2} = \int d\vec{\bar{\kappa}}_0 p(\vec{\bar{\kappa}}_0) \rho_1^{(\vec{\bar{\kappa}}_0)} \otimes \rho_2^{(-\vec{\bar{\kappa}}_0)}, \tag{31}$$

where $\rho_1^{(\vec{\bar{\kappa}}_0)}$ and $\rho_2^{(-\vec{\bar{\kappa}}_0)}$ are the density matrices associated with the single-photon pure states of Eq. (30).

The system described by Eq. (31) represents the "classical" (i.e., entanglement-free) simulation of the SPDC signal-idler pairs. Different from entangled two-photon states, this classical source emits pairs of independent photons, each one with a well-defined momentum [25]. The uncertainty characterizing the momentum of each photon is equal to the variance of the single-photon probability distribution $|f|^2$ of Eq. (30). Therefore, when this source is used in the setup of Fig. 4, the double-arrowed straight lines assume a very different meaning with respect to the SPDC case: each line represents a pair of independent photons and is emitted by the source with probability $p(\vec{\bar{\kappa}}_0)$, at different times.

For the separable system of Eq. (31), if photons 1 propagate in arm a and photons 2 in arm b, the second-order correlation function defined in Eq. (11) reduces to

$$G^{(2)}(\vec{\rho}_1, \vec{\rho}_2) = \int d\vec{\bar{\kappa}}_0 p(\vec{\bar{\kappa}}_0) \times \left| \int d\vec{\kappa}_1 f_1(\vec{\kappa}_1 - \vec{\bar{\kappa}}_0) g_a(\vec{\kappa}_1, \omega; \vec{\rho}_1, z_a) \right|^2 \times \left| \int d\vec{\kappa}_2 f_2(\vec{\kappa}_2 + \vec{\bar{\kappa}}_0) g_b(\vec{\kappa}_2, \omega; \vec{\rho}_2, z_b) \right|^2. \tag{32}$$

Hence, the second-order correlation function is given by the weighted sum (over all photon pairs) of the products of the probability distribution associated with photon 1 (propagating in arm a) times the probability distribution associated with photon 2 (propagating in arm b). The result of Eq. (32) is very different from the one obtained for the SPDC entangled two-photon system, where the second-order correlation function was given by the modulus square of the biphoton amplitude [Eq. (17)]. Does this mean that coincidence measurements performed in the optical setup of Fig. 4 will give different results when the SPDC source is replaced by the classical statistical mixture of Eq. (31)? In order to answer this question, we will now evaluate the second-order correlation function for the setup of Fig. 4, considering the incoherent statistical mixture of Eq. (31) as the source.

When detector D_a measures the momentum of photons 1 [Eq. (13)] and detector D_b detects photons 2 in an arbitrary plane [Eq. (15)], we have

$$G^{(2)}(\vec{\rho}_1,\vec{\rho}_2)_{(MOM)} = C\int d\vec{\bar{\kappa}}_0 p(\vec{\bar{\kappa}}_0)\left|\int d\vec{\kappa}_1 f_1(\vec{\kappa}_1-\vec{\bar{\kappa}}_0)G(|\vec{\kappa}_1|)_{[-cd_a/\omega]}\tilde{T}\left(\vec{\kappa}_1-\frac{\omega}{cf_{coll}}\vec{\rho}_1\right)\right|^2$$
$$\times\left|\int d\vec{\kappa}_2 f_2(\vec{\kappa}_2+\vec{\bar{\kappa}}_0)G(|\vec{\kappa}_2|)_{[-cd_b/\omega]}\int d\vec{\rho}_l G(|\vec{\rho}_l|)_{[(\omega/c)(1/d_b'-1/f)]}e^{i\{\vec{\kappa}_2-[\omega/(cd_b')]\vec{\rho}_2\}\cdot\vec{\rho}_l}\right|^2. \quad (33)$$

By implementing a momentum-momentum measurement (i.e., taking $d_b'=f$), the second-order correlation function gives

$$G^{(2)}(\vec{\rho}_1,\vec{\rho}_2)_{(MOM)} \approx C\int d\vec{\bar{\kappa}}_0 p(\vec{\bar{\kappa}}_0)\left|f_2\left(\frac{\omega}{cf}\vec{\rho}_2+\vec{\bar{\kappa}}_0\right)\right|^2$$
$$\times\left|\int d\vec{\kappa}_1 f_1(\vec{\kappa}_1-\vec{\bar{\kappa}}_0)G(|\vec{\kappa}_1|)_{[-cd_a/\omega]}\right.$$
$$\left.\times\tilde{T}\left(\vec{\kappa}_1-\frac{\omega}{cf_{coll}}\vec{\rho}_1\right)\right|^2. \quad (34)$$

Therefore, if the object is completely covered by the one-photon beam and the function $f_1(\vec{\kappa}_1-\vec{\bar{\kappa}}_0)$ is narrow enough (i.e., it approximates a δ function), the Fourier transform of the object can be reproduced by the second-order correlation function. For this to be a ghost interference-diffraction pattern, the probability distribution $p(\vec{\bar{\kappa}}_0)$ needs to be wide enough to erase any first-order effect from the plane of detector D_1.

The incoherence of the source is reflected in the result of Eq. (34): the coincidence counts are given by the *weighted* sum of the hidden first-order effect (given by the modulus square of the convolution between the Fourier transform of the object $\tilde{T}$ and the single-photon probability amplitude f_1) with the "single-photon" transverse probability distribution $|f_2|^2$. This result is clearly different from the one found for the SPDC two-photon system [see Eq. (19)]. However, in the plane-wave approximation, we find $G^{(2)}(\vec{\rho}_1,\vec{\rho}_2)_{(MOM)}\propto|\bar{T}[\vec{\bar{\kappa}}_0-\vec{\rho}_1\omega/(cf_{coll})]|^2$, which is exactly the same result we obtained for the momentum-momentum correlation measurement realized on the SPDC signal-idler pairs generated by a plane-wave pump beam.

With the appropriate choice of the probability distributions $|f_{1,2}|^2$ and $p(\vec{\bar{\kappa}}_0)$, the uncertainty in $\vec{\kappa}_1+\vec{\kappa}_2$ can be made quantitatively equal to the one obtained for the SPDC source [Eq. (18)]. This result is consistent with our initial assumption: the source under investigation is characterized by classical statistical correlation in transverse momentum. However, based on Eq. (34), the visibility of the ghost interference-diffraction pattern is affected by the variances of both the single-photon probability amplitudes f_1 and f_2. Therefore, the uncertainty $\Delta(\vec{\kappa}_1+\vec{\kappa}_2)$ has a lower bound given by

$$\Delta(\vec{\kappa}_1+\vec{\kappa}_2)=\sqrt{\sigma_1^2+\sigma_2^2}=\sqrt{2}\sigma,$$

in agreement with the first EPR inequality for separable systems given in Eq. (10). This is a consequence of the intrinsic independence of photons 1 and 2 of each pair of the ensemble and explicitly demonstrates that photons 1 and photons 2 are diffracted separately, independently of each other.

Now consider the case in which D_a is a bucket detector implementing position measurement in arm a [Eq. (14)], while detector D_b scans an arbitrary plane of arm b [Eq. (15)]. The second-order correlation function of Eq. (32) becomes

$$G^{(2)}(\vec{\rho}_1,\vec{\rho}_2)_{(POS)} = C\int d\vec{\bar{\kappa}}_0 p(\vec{\bar{\kappa}}_0)\left|\int d\vec{\rho}_o t(\vec{\rho}_o)e^{-i[\omega/(cf_{coll})]\vec{\rho}_1\cdot\vec{\rho}_o}\int d\vec{\kappa}_1 f_1(\vec{\kappa}_1-\vec{\bar{\kappa}}_0)G(|\vec{\kappa}_1|)_{[-cd_a/\omega]}e^{i\vec{\kappa}_1\vec{\rho}_o}\right|^2$$
$$\times\left|\int d\vec{\kappa}_2 f_2(\vec{\kappa}_2+\vec{\bar{\kappa}}_0)G(|\vec{\kappa}_2|)_{(-(c/\omega)\{d_b+[(1/(1/d_b'-1/f)]\})}\right)\exp\left(i\vec{\kappa}_2\cdot\frac{\vec{\rho}_2}{1-\frac{d_b'}{f}}\right)\right|^2, \quad (35)$$

where we assumed the lens to have infinite transverse dimension. Equation (35) does not lead to any thin-lens equation and clearly indicates the absence of position-position correlation. In fact, even after integrating over the area of the bucket detector D_a, we have

$$G^{(2)}(A_{obj},\vec{\rho}_2)_{(POS)} = C\int d\vec{\bar{\kappa}}_0 p(\vec{\bar{\kappa}}_0)\left|\int d\vec{\kappa}_2 f_2(\vec{\kappa}_2+\vec{\bar{\kappa}}_0)G(|\vec{\kappa}_2|)_{(-(c/\omega)\{d_b+[1/(1/d_b'-1/f)]\})}\exp\left(i\vec{\kappa}_2\cdot\frac{\vec{\rho}_2}{1-\frac{d_b'}{f}}\right)\right|^2$$
$$\times\int d\vec{\rho}_o|t(\vec{\rho}_o)|^2\left|\int d\vec{\kappa}_1 f_1(\vec{\kappa}_1-\vec{\bar{\kappa}}_0)G(|\vec{\kappa}_1|)_{[-cd_a/\omega]}e^{i\vec{\kappa}_1\vec{\rho}_o}\right|^2; \quad (36)$$

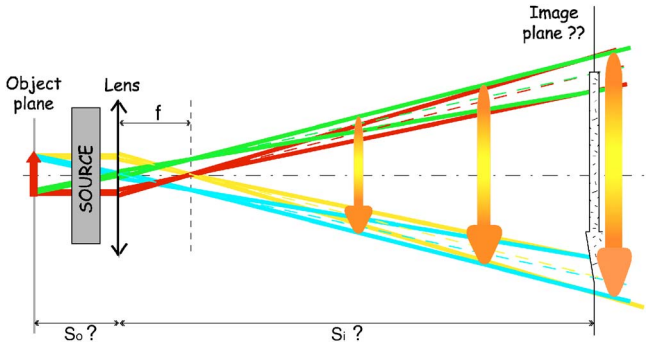

FIG. 5. (Color online) The source emits pairs of photons in a classical statistical mixture that simulates the SPDC entangled two-photon system. The average momenta (dashed lines) of photons 2 intersect in the plane at distance s_i from the lens, but the spread in the momenta of photons 2 (diverging continuous lines) is such that no image plane can be defined neither theoretically nor experimentally. Only projections (shaded arrows) can be observed. Also notice that, due to the dimensions of the single-photon beams compared to the object size, this source does not allow reproducing the Fourier transform of the object.

i.e., the coincidence counts are unable to reconstruct the object transfer function and no image can be observed.

It is interesting to notice that, when $f_{1,2}$ are narrow enough for the momentum-momentum measurement described by Eq. (34) to reproduce the ghost Fourier transform of the object, the joint probability distribution of Eq. (36) is approximately constant. The opposite situation is drawn in the pictorial representation of Fig. 5: wide probability distributions $f_{1,2}$ (i.e., narrow beams) may give rise to *projections* which partially reproduce the shape of the object, but in this case neither first- nor second-order interference-diffraction patterns of the aperture is defined.

These results are in good agreement with the results found in Secs. II B and II C: for separable systems of quanta (here photons), the higher the accuracy characterizing moment-momentum correlation measurements, the lower the accuracy achievable in position-position correlation measurements (and vice versa). And in fact, based on Eq. (36), we find $\Delta(\vec{\rho}_1-\vec{\rho}_2)\geqslant 1/2\sqrt{1/\sigma_1^2+1/\sigma_2^2}$, in agreement with the second EPR inequality for separable systems of Eqs. (10).

We conclude that a separable system of classically correlated photons can reproduce only one feature of the SPDC two-photon pairs: the anticorrelation in transverse momentum and, consequently, the ghost interference-diffraction pattern. However, due to the absolute incoherence characterizing this source, the classical anticorrelation in momentum is not accompanied by correlation in position: no thin-lens equation can be found and, consequently, no ghost image can ever be observed [37].

VI. GHOST IMAGING WITH THERMAL LIGHT

We now consider another example of classical optical source [25]: a source of chaotic thermal light. Thermal sources have recently been proposed [18,19] as possible candidates for reproducing certain features of quantum ghost imaging effects. Several imaging experiments with pseudo-thermal radiation have been realized in our laboratory [22,23,38] and, independently, by Magatti *et al.* [24]. In particular, a "thermal two-photon thin-lens equation" was theoretically proposed in both [21,23] and experimentally verified in our laboratory [23]. Furthermore, the experimental work of Magatti *et al.* [24] reported a ghost image and interference experiment realized with thermal light. The results of this experiment have been used to claim that thermal light can violate an inequality somewhat similar to Eq. (9). This violation would be in contradiction with many theoretical [26] and experimental [11,17] works which proved that such an inequality is a necessary condition for separability. In fact, as we will explicitly prove, the conclusions drawn in [24] derive from an incorrect evaluation of the uncertainties involved in the inequality.

In this section we will briefly review the theoretical derivation of both the thermal thin-lens equation and the thermal ghost interference-diffraction pattern, considering a thermal source in the EPR-type experimental setup of Fig. 4. We will then focus on the accuracy of thermal ghost imaging and compare it with the one characterizing quantum ghost imaging.

For thermal sources, the second-order correlation function of Eq. (11) reduces to the summation of the products of intensities (i.e., first-order correlation functions) [19,30,39]:

$$G^{(2)}(\vec{r}_1,\vec{r}_2,t_1,t_2)=G_{11}^{(1)}G_{22}^{(1)}+|G_{12}^{(1)}(\vec{r}_1,\vec{r}_2;t_1-t_2)|^2, \quad (37)$$

where [18,19,23]:

$$G_{ij}^{(1)}(\vec{r}_i,\vec{r}_j;t_i-t_j)=\int d\vec{\kappa}\int d\omega g_i^*(\vec{\kappa},\omega;\vec{\rho}_i,z_i)g_j(\vec{\kappa},\omega;\vec{\rho}_j,z_j)\times\langle n_\omega\rangle e^{i\omega(t_i-t_j)}, \quad (38)$$

for $i,j=1,2$; $\langle n_\omega\rangle=(e^{\hbar\omega/(K_BT)}-1)^{-1}$ is the average photon number at temperature T. The second-order correlation function for chaotic thermal light has a peculiar functional form: the first term of Eq. (37) represents a constant background noise, given by the product of the intensities at the two detectors (D_1 and D_2, respectively); the second term is the modulus square of the first-order correlation function measured by the two spatially separated detectors. In other words, no second-order coherence exists. The term $g_1^*g_2$ of Eq. (38) indicates that the second term of Eq. (37) is the result of an interference. In order to emphasize the similarity with the SPDC biphoton amplitude, which contains a g_1g_2 term, we may regard this interference as a *coherent superposition of the probability amplitudes associated with two spatially separated optical arms*. Hence, despite the fact that thermal sources are incoherent sources, thermal second-order effects may be seen, in part, as the result of the coherent superposition of two-photon probability amplitudes [23,38]. It is then reasonable to expect that coincidence experiments realized with thermal light, in the setup of Fig. 4, might reproduce the results found in Sec. IV for SPDC entangled two-photon pairs. Notice, however, that the constant background noise reflects the very different physics governing thermal sources [12,19] and, in particular, their incoherent nature. Furthermore, the fact that the thermal two-photon

probability amplitude has the functional form $g_1^* g_2 \langle n \rangle$, reminds us that the coupling between arm 1 and arm 2 is the result of an "intensity" measurement, rather than a pure second-order effect.

To better understand the analogies and differences between the experimental results obtained with thermal and SPDC sources, we will now evaluate the second-order correlation function describing a thermal source in the setup of Fig. 4. Differently from the previous cases, the finite size of the pump beam will now be taken into account through the fields, rather than the state of the source; by reevaluating the transfer functions g_a and g_b for the same optical setup described by Eq. (13) [or Eq. (14)] and Eq. (15), but taking into account the finite transverse area of the source, we find (see the Appendix)

$$g_a(\vec{\kappa},\omega;\vec{\rho}_a,z_a=d_a+f_{coll}) = \frac{-\omega^2 e^{i(\omega/c)z_a}}{(2\pi c)^2 d_a f_{coll}} G(|\vec{\rho}_a|)_{[\omega/(cf_{coll})]} \times \int_{A_{obj}} d\vec{\rho}_o t(\vec{\rho}_o) G(|\vec{\rho}_o|)_{[\omega/(cd_a)]} e^{-i[\omega/(cf_{coll})]\vec{\rho}_o\cdot\vec{\rho}_a} \times \int_{A_{source}} d\vec{\rho}_x f(\vec{\rho}_x) G(|\vec{\rho}_x|)_{[\omega/(cd_a)]} e^{i\{\vec{\kappa}-[\omega/(cd_a)]\vec{\rho}_o\}\cdot\vec{\rho}_x} \tag{39}$$

and

$$g_b(\vec{\kappa},\omega;\vec{\rho}_b,z_b=d_b+d_b') = \frac{-\omega^2 e^{i(\omega/c)z_b}}{(2\pi c)^2 d_b d_b'} G(|\vec{\rho}_b|)_{[\omega/(cd_b')]} \times \int_{A_{source}} d\vec{\rho}_x f(\vec{\rho}_x) G(|\vec{\rho}_x|)_{[\omega/(cd_b)]} e^{i\vec{\kappa}\cdot\vec{\rho}_x} \times \int_{A_{lens}} d\vec{\rho}_l G(|\vec{\rho}_l|)_{[(\omega/c)(1/d_b+1/d_b'-1/f)]} \times \exp\left[-i\frac{\omega}{c}\left(\frac{\vec{\rho}_x}{d_b}+\frac{\vec{\rho}_b}{d_b'}\right)\cdot\vec{\rho}_l\right], \tag{40}$$

where $f(\vec{\rho}_x)$ describes the finite source aperture.

Let us start by considering the case of a momentum-momentum measurement: the fields at the detectors are related to the transfer functions of Eqs. (39) and (40), with $d_b'=f$. By plugging in these expressions into Eq. (38), we find

$$G^{(2)}(\vec{\rho}_1,\vec{\rho}_2,T_1,T_2)_{(MOM)} = G_{11}^{(1)}G_{22}^{(1)} + \left| \int d\omega S_\omega(\vec{\rho}_1,\vec{\rho}_2,T_1-T_2) \times \int d\vec{\kappa}\widetilde{T}\left(\vec{\kappa}-\frac{\omega}{cf_{coll}}\vec{\rho}_1\right) \times \widetilde{F}^2\left(\vec{\kappa}-\frac{\omega}{cf}\vec{\rho}_2\right) G(|\vec{\kappa}|)_{[cd_a/\omega]} \right|^2, \tag{41}$$

where the first term represents a background noise, given by the product of the intensities at each detector:

$$G_{11}^{(1)} \propto \int d\omega \langle \bar{n}_\omega \rangle \frac{\omega^4}{(2\pi c)^4 f_{coll}^2 d_a^2} \int d\vec{\rho}_x |f(\vec{\rho}_x)|^2 \times \left| \int d\vec{\rho}_o t(\vec{\rho}_o) G(|\vec{\rho}_o|)_{[\omega/cd_a]} \times \exp\left[-i\frac{\omega}{c}\left(\frac{\vec{\rho}_x}{d_a}+\frac{\vec{\rho}_1}{f_{coll}}\right)\cdot\vec{\rho}_o\right] \right|^2 \approx \int d\omega \langle \bar{n}_\omega \rangle \omega^2 \int d\vec{\rho}_o |t(\vec{\rho}_o)|^2,$$

$$G_{22}^{(1)} \propto \int d\omega \langle \bar{n}_\omega \rangle \omega^2 \int d\vec{\rho}_x |f(\vec{\rho}_x)|^2. \tag{42}$$

The analogy between the SPDC result of Eq. (19) and the second term of Eq. (41) is quite interesting. First of all, we notice that, similarly to the SPDC case [see Eq. (18)], the transverse spatial correlation can only be observed by counting coincidences within the "coherence time" characterizing thermal radiation, given by the frequency integral of

$$S_\omega(\vec{\rho}_1,\vec{\rho}_2,T_1-T_2) = \langle \bar{n}_\omega \rangle \frac{-\omega^2}{(2\pi c)^2 f f_{coll}} \exp\left(i\omega \left\{ T_1 - T_2 - \frac{1}{2c}\left[\frac{|\vec{\rho}_1|^2}{f_{coll}} - \frac{|\vec{\rho}_2|^2}{f}\left(1-\frac{d_b}{f}\right)\right]\right\}\right). \tag{43}$$

Furthermore, the transverse spatial part of the second term of Eq. (41) indicates that, when detector D_a is fixed in the far field of the object and detector D_b scans the focal plane of the imaging lens, the Fourier transform of the object transfer function ($\widetilde{T}$) is reproduced by the coincidence counts. Similar to the SPDC case, the resulting pattern is given by the convolution of the Fourier transform of the object ($\widetilde{T}$) with the angular distribution of the thermal radiation [$\widetilde{F}^2=\mathrm{FT}(|f|^2)$] and the envelope of the radiation on the aperture plane (G).

Based on Eq. (42), the single counts at both detectors are constant: no first-order effect exists. Therefore, thermal sources give rise to ghost interference-diffraction. However, due to the first term of Eq. (41), the thermal ghost interference-diffraction pattern lays over a constant background noise extending (after normalization) from 0 to 1; the maximum achievable visibility of the thermal ghost interference-diffraction pattern is only 33%.

Some important differences between the $G_{MOM}^{(2)}$ obtained for thermal, classically correlated, and entangled (SPDC) systems deserve to be emphasized. First, we notice that, while for both SPDC and classically correlated photon pairs the second-order correlation function depends on $\vec{\kappa}_1+\vec{\kappa}_2$, for thermal light it depends on $\vec{\kappa}_1-\vec{\kappa}_2$. This is due to the fact that SPDC radiation is intrinsically characterized by anticorrelation in transverse momentum, and classically correlated photon pairs were built in such a way to simulate the same anticorrelation; however, thermal effects are the result of the self-correlation of each mode of the thermal radiation with itself.

Of particular interest is the fact that, based on the probability distribution of the coincidence counts found in Eq. (41), the uncertainty in $\vec{\kappa}_1-\vec{\kappa}_2$ is given by

$$\Delta(\vec{\kappa}_1-\vec{\kappa}_2)=\sqrt{\Delta(\vec{\kappa}_1-\vec{\kappa}_2)_{BACK}^2+\Delta(\vec{\kappa}_1-\vec{\kappa}_2)_{PEAK}^2},$$

i.e., is the sum of the uncertainty characterizing the constant background plus the uncertainty characterizing the peak $|G_{12}^{(1)}|^2$. Since the background is given by the product of the intensities at detectors D_1 and D_2, we have $\Delta(\vec{\kappa}_1-\vec{\kappa}_2)_{BACK}=\sqrt{\Delta(\vec{\kappa}_1)^2+\Delta(\vec{\kappa}_2)^2}$, which, based on Eqs. (42), is very large; then,

$$\Delta(\vec{\kappa}_1-\vec{\kappa}_2)=\sqrt{\Delta(\vec{\kappa}_1)^2+\Delta(\vec{\kappa}_2)^2+\Delta(\vec{\kappa}_1-\vec{\kappa}_2)_{PEAK}^2}\approx\sqrt{\Delta(\vec{\kappa}_1)^2+\Delta(\vec{\kappa}_2)^2}\approx\infty. \quad (44)$$

Therefore, within a very good approximation, thermal sources satisfy the inequalities of Sec. II B for independent quanta. This result is a consequence of both the lack of correlation and the intrinsic incoherence of thermal light.

It is quite interesting to compare the result found here with the one obtained in Sec. V, where we have seen that the ghost Fourier transform of the object can only be observed when the classically correlated pairs of photons are characterized by a small uncertainty $\Delta(\vec{\kappa}_1+\vec{\kappa}_2)$ [see Eq. (34)]. From this perspective, it is quite surprising that thermal sources, which are characterized by the lack of correlations [as indicated by Eq. (44)], give rise to a ghost interference-diffraction pattern, as well. However, the Fourier transform of the object appearing in the thermal coincidence counts may be regarded as the result of the coherent superposition of two-photon amplitudes. In other words, the classical Sec. V simulates the momentum-momentum correlation of entangled two-photon systems but cannot simulate the coherent superposition; a chaotic thermal source, on the contrary, simulates the coherent superposition of two-photon amplitudes. In both cases the quantum ghost interference-diffraction pattern can be simulated, even if the functional forms are very different in the two cases.

Let us now consider the case of a position-position measurement realized on thermal light in the setup of Fig. 4. By substituting the expressions for the transfer functions given by Eqs. (39) and (40) in Eq. (38) and performing the integrations over transverse momenta and imaging lens, we find, for the spatial part,

$$G_{12}^{(1)}(\vec{\rho}_1,\vec{\rho}_2)_{(POS)}\propto\int d\vec{\rho}_o t^*(\vec{\rho}_o)G(|\vec{\rho}_o|)_{[-\omega/(cd_a)]}e^{i[\omega/(cf_{coll})]\vec{\rho}_1\cdot\vec{\rho}_o}\int d\vec{\rho}_x|f(\vec{\rho}_x)|^2G(|\vec{\rho}_x|)_{((\omega/c)(1/d_b-1/d_a-(1/d_b)\{1/[1+d_b(1/d_b'-1/f)]\}))}$$
$$\times\exp\left[-i\frac{\omega}{c}\left(\frac{\vec{\rho}_2}{d_b'd_b(1/d_b+1/d_b'-1/f)}-\frac{\vec{\rho}_o}{d_a}\right)\vec{\rho}_x\right], \quad (45)$$

where the imaging lens has been assumed to have infinite transverse dimension. The argument of the integral over the source indicates the existence of a "two-photon thin lens equation" [21,23]: $1/s_o+1/s_i=1/f$, with $s_o=d_b-d_a$ and $s_i=d_b'$. In the two-photon image plane defined by this thin-lens equation, the second-order spatial correlation function reduces to

$$G^{(2)}(A_{obj},\vec{\rho}_2,t_1,t_2)_{(POS)}\propto G_{11}^{(1)}G_{22}^{(1)}+\int d\vec{\rho}_o|t(\vec{\rho}_o)|^2\times\left|\tilde{F}^2\left[\frac{\omega}{cd_a}\left(\frac{\vec{\rho}_2}{m}-\vec{\rho}_o\right)\right]\right|^2, \quad (46)$$

where $m=-s_i/s_o$ and the intensities at the two detectors are

$$G_{11}^{(1)}\propto\int d\vec{\rho}_1\int d\vec{\rho}_x|f(\vec{\rho}_x)|^2\left|\tilde{T}\left[\frac{\omega}{c}\left(\frac{\vec{\rho}_x}{d_a}+\frac{\vec{\rho}_1}{f_{coll}}\right)\right]\right|^2,$$

$$G_{22}^{(1)}\propto\int d\vec{\rho}_x|f(\vec{\rho}_x)|^2. \quad (47)$$

Equation (46) indicates that, whenever D_a is a fixed bucket detector and D_b scans the image plane defined by the two-photon thin-lens equation found above, the coincidence counts reproduce the ghost image of the object, magnified by a factor of $m=-s_i/s_o$ [21,23]. This image is accompanied by a constant background noise, given by the product of the intensities at detectors D_1 and D_2. The existence of a two-photon thin lens equation may again be regarded as the result of the coherent superposition of two-photon amplitudes. Similarly to the SPDC case, the image is given by the convolution of the object transfer function with the angular spectrum of the thermal radiation ($\tilde{F}^2$); this result is due to the fact that we considered the imaging lens to have infinite transverse dimension. When the finite dimension of the imaging lens is taken into account, the function $P[\omega/cX_{NA}(\vec{\rho}_2/m-\vec{\rho}_o)]$ (with $X_{NA}=R_{lens}/s_o$) also appears in the argument of the integral over the object.

Regarding the position-position EPR-type correlation measurement, the first noticeable difference between thermal sources and SPDC two-photon systems is the two-photon thin-lens equation. For SPDC, the object (or image) distance is $s_o=d_a+d_b$, while for thermal photons it is $s_o=d_b-d_a$. The practical consequences of this results are discussed in [21,23]. However, the most important difference between quantum and thermal ghost images is given by the values of the uncertainties in $\vec{\rho}_1-\vec{\rho}_2$—i.e., by the resolution. Following the same argument that brought us to write Eq. (44), we find

$$\Delta(\vec{\rho}_1-\vec{\rho}_2)=\sqrt{\Delta(\vec{\rho}_1)^2+\Delta(\vec{\rho}_2)^2+\Delta(\vec{\rho}_1-\vec{\rho}_2)^2_{PEAK}}$$
$$\approx\sqrt{\Delta(\vec{\rho}_1)^2+\Delta(\vec{\rho}_2)^2}, \quad (48)$$

with $\Delta(\vec{\rho}_1)=A_{obj}$ and $\Delta(\vec{\rho}_2)\approx\infty$, both of which are much larger than the uncertainty:

$$\Delta(\vec{\rho}_1-\vec{\rho}_2)_{PEAK}=\sqrt{\frac{1}{2\sigma^2}+\left(\frac{1.22\lambda}{X_{NA}}\frac{2}{2}\right)^2}, \quad (49)$$

where σ_s^2 is the variance of the source-size function $f(\vec{\rho})$. In summary, similarly to entangled systems [see Eq. (23)], thermal sources can reproduce a ghost image [see Eq. (46)]; however, due to the significant background noise, thermal sources can never achieve the same high resolution [compare Eq. (48) with Eq. (24)]. Notice, for instance, that the function $\tilde{F}^2$, alone, can no more be regarded as two-photon point-spread functions: the two-photon point-spread function for chaotic thermal radiation also contains the constant background noise.

It is interesting to notice that, in the thermal case, complicated objects give rise to a larger background noise; therefore, well-resolved thermal ghost images of complicated objects are always characterized by a decreased visibility [21,23]. In other words, for thermal sources, high visibility and high resolution are incompatible. This effect is exclusively due to the presence of a constant background noise. Therefore, from a point of view of practical applications, it would be useful to find a detection scheme which is capable of subtracting the background noise. In fact, *after removal of the constant background*, the resolution of the thermal ghost image may become comparable to the one achieved by entangled states [compare Eq. (24) with Eq. (49)]. Such a detection scheme would lead the way toward the application of thermal sources for high-accuracy nonlocal positioning.

From a fundamental physics perspective, the role of the constant background noise is essential: it is a manifestation of the different physics governing entangled and thermal sources. In fact, the constant background determines the values of the uncertainties $\Delta(\vec{\kappa}_1-\vec{\kappa}_2)$ and $\Delta(\vec{\rho}_1-\vec{\rho}_2)$, thus guaranteeing that the uncertainty relation $\Delta(\vec{\kappa}_1-\vec{\kappa}_2)\Delta(\vec{\rho}_1-\vec{\rho}_2)\geqslant 1$ is satisfied.

In this respect, it is worth pointing out that Magatti *et al.* [24] have drawn an incorrect conclusion by claiming a violation, for thermal light, of the separability condition $\Delta x_2|_1\,\Delta k_{x2}|_1\geqslant 1$ [26]. In fact, Magatti *et al.* evaluated the conditional uncertainties $\Delta\, x_2|_1$ and $\Delta\, k_{x2}|_1$ (which characterize the measurement of x_2 and k_{x2} conditioned by the measurement of x_1 and k_{x1}, respectively) by considering only the "peak" of the second-order correlation function for thermal radiation—i.e., subtracting the significant constant background noise from the measured joint probability distribution. This led them to conclude that thermal radiation can violate the separability condition reported above. The violation never occurs if the whole measured joint probability distribution $G^{(2)}$ is taken into account, as it should. Furthermore, since, for thermal radiation, the conditional uncertainties are $\Delta\, x_2|_1=\Delta(x_1-x_2)$ and $\Delta\, k_{x2}|_1=\Delta(k_{x1}-k_{x2})$, and since (x_1-x_2) and $(k_{x1}-k_{x2})$ are conjugate variables, the result presented in [24] (namely, $\Delta\, x_2|_1\Delta\, k_{x2}|_1<1$) would in fact represent a violation of the uncertainty relation.

VII. SUMMARY AND CONCLUSION

We have proposed an operational approach for the implementation of momentum-momentum and position-position correlation measurements on systems of photons. Through the evaluation of the second-order correlation function $G^{(2)}(\vec{\rho}_1,z_1;\vec{\rho}_2,z_2)$ associated with EPR-type ghost imaging setups, we have quantified the uncertainties $\Delta(\vec{\kappa}_1\pm\vec{\kappa}_2)$ and $\Delta(\vec{\rho}_1-\vec{\rho}_2)$ for entangled photon pairs, for classically correlated photons, and for thermal light. Both $\Delta(\vec{\kappa}_1\pm\vec{\kappa}_2)$ and $\Delta(\vec{\rho}_1-\vec{\rho}_2)$ have a precise operational meaning: they are related to the resolution and the visibility of ghost imaging patterns.

Entangled two-photon systems are characterized by two peculiar properties: (1) coherent superposition of two-photon amplitudes and (2) correlation in both momentum and position variables. Both these properties give rise to ghost images whose resolution may only be limited by the finite numerical aperture of the image forming system. In principle, quantum ghost imaging can achieve 100% visibility.

It is worth emphasizing that the classical Rayleigh diffraction limit does not necessarily impose a limit on entangled two-photon systems: with an adequate choice of the experimental setup (see [6,7]), entangled two-photon systems can overcome the Rayleigh diffraction limit and give rise to super-resolved optical images, still characterized by 100% visibility.

Separable systems of photons may simulate only one of the two distinctive properties of entangled states. Therefore, only one aspect of quantum ghost imaging effects can be reproduced by classical sources [25]. In particular, separable systems of photon pairs can simulate the momentum-momentum correlation and, consequently, the ghost interference-diffraction effect. Under certain experimental conditions, entangled and classically correlated photon pairs can give rise to the same quantitative value of the uncertainty $\Delta(\vec{\kappa}_1+\vec{\kappa}_2)$. However, separable systems of photon pairs are intrinsically incoherent and the correlation in momentum is not sufficient to produce the position-position correlation required to generate a ghost image.

On the other hand, chaotic thermal sources give rise to a sort of coherent superposition of two-photon amplitudes; they can then reproduce both ghost interference-diffraction and ghost images, but always accompanied by a significant background noise. The uncertainties in both $\Delta(\vec{\kappa}_1-\vec{\kappa}_2)$ and $\Delta(\vec{\rho}_1-\vec{\rho}_2)$ are considerably large, and their product is much larger than the limit imposed by the uncertainty relation. Furthermore, the results of Eqs. (44) and (48) indicate that chaotic thermal sources are characterized by the lack of correlation both in momentum and in position. The constant background noise imposes stringent limitations on the visibility (max 33%) and the overall resolution of thermal ghost images. However, as far as practical applications are concerned, thermal sources are interesting candidates for high-accuracy nonlocal positioning; such applications rely on the

development of detection schemes which are capable of eliminating the constant background.

ACKNOWLEDGMENTS

The authors thank Giuliano Scarcelli and Sulakshana Thanvanthri for helpful and stimulating discussions. This research was supported in part by NSF, ONR, and the NASA-CASPR program.

APPENDIX: EVALUATION OF THE FIELD OPERATORS AT THE DETECTORS

In this appendix we wish to prove the validity of Eqs. (13)–(15) for the fields at the detectors in the setup drawn in Fig. 4. We will start from the evaluation of the optical transfer functions (g_a and g_b) for arms a and b and we will plug the results in the generic expression of the field given in Eq. (12); the paraxial approximation will be used everywhere.

The optical transfer function describing arm a of the setup of Fig. 4 is given by [31,32]

$$\begin{aligned} g_a(\vec{\kappa},\omega;\vec{\rho}_a,z_a=d_a+d_a') &= \int_{A_{source}} d\vec{\rho}_x \int_{A_{obj}} d\vec{\rho}_o \\ &\times \left\{ \frac{-i\omega}{2\pi c d_a} e^{i\vec{\kappa}\cdot\vec{\rho}_x} e^{i(\omega/c)d_a} G(|\vec{\rho}_x-\vec{\rho}_o|)_{[\omega/(cd_a)]} \right\} \\ &\times t(\vec{\rho}_o) \left\{ \frac{-i\omega}{2\pi c d_a'} e^{i(\omega/c)d_a'} G(|\vec{\rho}_o-\vec{\rho}_a|)_{[\omega/(cd_a')]} \right\}, \end{aligned} \tag{A1}$$

where $\vec{\rho}_x$ and $\vec{\rho}_o$ are two-dimensional vectors defined, respectively, on the (transverse) output plane of the source and on the object plane; the function $G(|\alpha|)_{[\beta]}$ is a Gaussian in $|\alpha|$, whose imaginary variance is related to the parameter $\beta[G(|\alpha|)_{[\beta]}=e^{i\beta/2|\alpha|^2}]$; the function $t(\vec{\rho}_o)$ is the transmission function of the object. The terms in the first and second curly brackets of Eq. (A1) describe free space propagation from the output plane of the source to the object plane and from the object plane to the detection plane, respectively.

The Gaussian function $G(|\alpha|)_{[\beta]}$ satisfies the following properties [31,32]:

$$\begin{aligned} G^*(|\vec{\alpha}|)_{[\beta]} &= G(|\vec{\alpha}|)_{[-\beta]}, \\ G(|\vec{\alpha}|)_{[\beta+\beta']} &= G(|\vec{\alpha}|)_{[\beta]} G(|\vec{\alpha}|)_{[\beta']}, \\ G(|\vec{\alpha}+\vec{\alpha}'|)_{[\beta]} &= G(|\vec{\alpha}|)_{[\beta]} G(|\vec{\alpha}'|)_{[\beta]} e^{i\beta\vec{\alpha}\cdot\vec{\alpha}'}, \\ \int d\vec{\alpha} G(|\vec{\alpha}|)_{[\beta]} e^{i\vec{\gamma}\cdot\vec{\alpha}} &= i\frac{2\pi}{\beta} G(|\vec{\gamma}|)_{[-1/\beta]}. \end{aligned} \tag{A2}$$

Notice that the last equation in Eqs. (A2) is the Fourier transform of the $G(|\alpha|)_{[\beta]}$ function. As we shall see in the following, these properties are very useful in simplifying the calculations of the optical transfer functions $g(\vec{\kappa},\omega;\vec{\rho}_j,z_j)$.

By employing the second and third expressions given in Eqs. (A2), the optical transfer function of Eq. (A1) simplifies to

$$\begin{aligned} g_a(\vec{\kappa},\omega;\vec{\rho}_a,z_a=d_a+d_a') &= -\frac{\omega^2 e^{i(\omega/c)z_a}}{(2\pi c)^2 d_a d_a'} G(|\vec{\rho}_a|)_{[(\omega/cd_a')]} \\ &\times \int_{A_{obj}} d\vec{\rho}_o t(\vec{\rho}_o) G(|\vec{\rho}_o|)_{[(\omega/c)(1/d_a+1/d_a')]} e^{-i[\omega/(cd_a')]\vec{\rho}_o\cdot\vec{\rho}_a)} \\ &\times \int_{A_{source}} d\vec{\rho}_x G(|\vec{\rho}_x|)_{[\omega/(cd_a)]} e^{i\{\vec{\kappa}-[\omega/(cd_a)]\vec{\rho}_o\}\cdot\vec{\rho}_x}. \end{aligned} \tag{A3}$$

After using the last property of Eq. (A2) and further simplifying the result we obtain

$$\begin{aligned} g_a(\vec{\kappa},\omega;\vec{\rho}_a,z_a) &= -\frac{i\omega e^{i(\omega/c)z_a}}{2\pi c d_a'} G(|\vec{\kappa}|)_{[-cd_a/\omega]} G(|\vec{\rho}_a|)_{[\omega/(cd_a')]} \\ &\times \int_{A_{obj}} d\vec{\rho}_o t(\vec{\rho}_o) G(|\vec{\rho}_o|)_{[(\omega/c)(1/d_a')]} e^{i\{\vec{\kappa}-[\omega/(cd_a')]\vec{\rho}_a\}\cdot\vec{\rho}_o}, \end{aligned} \tag{A4}$$

where the area of the source has been taken to be infinite. This can be done anytime the finite size of the source is included in the state of the source. Substituting the result of Eq. (A4) in the expression of the field given in Eq. (12), we obtain the field at detector D_a:

$$\begin{aligned} E_a^{(+)}(\vec{\rho}_a,z_a;t_a) &= C\frac{-i\omega}{2\pi c d_a'} \int d\omega e^{-i\omega(t_a-z_a/c)} G(|\vec{\rho}_a|)_{[\omega/(cd_a')]} \\ &\times \int d\vec{\kappa} G(|\vec{\kappa}|)_{[-cd_a/\omega]} \int_{A_{obj}} d\vec{\rho}_o t(\vec{\rho}_o) G(|\vec{\rho}_o|)_{[(\omega/c)(1/d_a')]} \\ &\times e^{i\{\vec{\kappa}-[\omega/(cd_a')]\vec{\rho}_a\}\cdot\vec{\rho}_o} a_{\vec{k}}, \end{aligned} \tag{A5}$$

where we have assumed that only one polarization can be detected by D_a and we have taken slowly varying terms in ω outside the frequency integral.

Now, in order to implement momentum measurement on photons propagating in arm a of the setup of Fig. 4, we need to place the pointlike detector D_a in the far field of the object $[D^2\omega/(cd_a')\ll 1]$ or, equivalently, in the focal plane of a converging lens ($d_a'=f_{coll}$). We implement this last situation by multiplying the field $E_a^{(+)}(\vec{\rho}_a,z_a;t_a)$ of Eq. (A5) by the transmission function of a lens placed in the plane of the object $[l(|\vec{\rho}_o|)_{f_{coll}}=G(|\vec{\rho}_o|)_{[-\omega/(cf_{coll})]}]$. The field at detector D_a as given in Eq. (A5) becomes

$$\begin{aligned} E_a^{(+)}(\vec{\rho}_a,z_a=d_a+f_{coll};t_a)_{(MOM)} &= C\frac{-i\omega}{2\pi c f_{coll}} \int d\omega e^{-i\omega(t_a-z_a/c)} G(|\vec{\rho}_a|)_{[\omega/(cf_{coll})]} \\ &\times \int d\vec{\kappa} G(|\vec{\kappa}|)_{[-cd_a/\omega]} \tilde{T}\left(\vec{\kappa}-\frac{\omega}{cf_{coll}}\vec{\rho}_a\right) a_{\vec{k}}, \end{aligned} \tag{A6}$$

where $\tilde{T}$ is the Fourier transform of the object transfer function $t(\vec{\rho}_o)$. This is the result employed in Eq. (13).

On the other hand, by replacing the pointlike detector D_a with a "bucket detector," we can measure the position of all photons transmitted by the object, independently of their momenta. From the experimental point of view a bucket detector may be implemented by inserting a short-focal-length converging lens in the object plane and by placing the detector in its focus; the sensitive area of the detector needs to be large enough to collect a big portion of the radiation in the focal plane of the collection lens. Therefore, also in this case, the field in one point of detector D_a is given by

$$E_a^{(+)}(\vec{\rho}_a, z_a = d_a + f_{coll}; t_a)_{(POS)} = C\frac{-i\omega}{2\pi c f_{coll}} \int d\omega e^{-i\omega(t_a - z_a/c)} G(|\vec{\rho}_a|)_{[\omega/(cf_{coll})]} \times \int d\vec{\kappa} G(|\vec{\kappa}|)_{[-cd_a/\omega]} \tilde{T}\left(\vec{\kappa} - \frac{\omega}{cf_{coll}}\vec{\rho}_a\right) a_{\vec{k}}; \quad \text{(A7)}$$

the integration over the area of the detector will be done after evaluating the correlation function $G^{(2)}(\vec{\rho}_a, \vec{\rho}_b)$. The result of Eq. (A7) is reported in Eq. (14).

Let us now evaluate the optical transfer function describing arm b of the setup of Fig. 4:

$$g_b(\vec{\kappa}, \omega; \vec{\rho}_b, z_b = d_b + d_b') = \int_{A_{source}} d\vec{\rho}_x \int_{A_{lens}} d\vec{\rho}_l \times \left\{ \frac{-i\omega}{2\pi c d_b} e^{i\vec{\kappa}\cdot\vec{\rho}_x} e^{i(\omega/c)d_b} G(|\vec{\rho}_x - \vec{\rho}_l|)_{[\omega/(cd_b)]} \right\} \times l(|\vec{\rho}_l|)_f \left\{ \frac{-i\omega}{2\pi c d_b'} e^{i(\omega/c)d_b'} G(|\vec{\rho}_l - \vec{\rho}_b|)_{[\omega/(cd_b')]} \right\}, \quad \text{(A8)}$$

where $\vec{\rho}_l$ is a two-dimensional vector defined on the (transverse) plane of the imaging lens; all other variables are defined as before. Again, the terms in curly brackets describe free space propagation from the output plane of the source to the lens and from the lens to the detection plane, respectively; the function in between them is the transmission function of the imaging lens of focal length f. Using the properties of the G functions reported in Eq. (A2), we simplify Eq. (A8) to

$$g_b(\vec{\kappa}, \omega; \vec{\rho}_b, z_b = d_b + d_b') = \frac{-i\omega e^{i(\omega/c)z_b}}{2\pi c d_b'} G(|\vec{\rho}_b|)_{[\omega/(cd_b')]} G(|\vec{\kappa}|)_{[-cd_b/\omega]} \times \int_{A_{lens}} d\vec{\rho}_l G(|\vec{\rho}_l|)_{[(\omega/c)(1/d_b' - 1/f)]} e^{i\{\vec{\kappa} - [\omega/(cd_b')]\vec{\rho}_b\}\cdot\vec{\rho}_l}, \quad \text{(A9)}$$

where, again, the source has been taken to be infinite in the transverse direction. The expression for the field at detector D_b can now be obtained by inserting this result into Eq. (12); we get

$$E_b^{(+)}(\vec{\rho}_b, z_b; t_b) = C\frac{-i\omega}{2\pi c d_b'} \int d\omega e^{-i\omega(t_b - z_b/c)} G(|\vec{\rho}_b|)_{[\omega/(cd_b')]} \times \int d\vec{\kappa} G(|\vec{\kappa}|)_{[-cd_b/\omega]} \times \int_{A_{lens}} d\vec{\rho}_l e^{i\{\vec{\kappa} - [\omega/(cd_b')]\vec{\rho}_b\}\cdot\vec{\rho}_l} G(|\vec{\rho}_l|)_{[(\omega/c)(1/d_b' - 1/f)]} a_{\vec{k}}, \quad \text{(A10)}$$

where we have assumed that only one polarization can be detected by D_b and we have taken slowly varying terms in ω outside the frequency integral. This is the same result reported in Eq. (15).

[1] D. V. Strekalov, A. V. Sergienko, D. N. Klyshko, and Y. H. Shih, Phys. Rev. Lett. **74**, 3600 (1995).

[2] T. B. Pittman, Y. H. Shih, D. V. Strekalov, and A. V. Sergienko, Phys. Rev. A **52**, R3429 (1995); T. B. Pittman, D. V. Strekalov, D. N. Klyshko, M. H. Rubin, A. V. Sergienko, and Y. H. Shih, *ibid.* **53**, 2804 (1996).

[3] The pioneering work of P. H. S. Ribeiro *et al.* [Phys. Rev. A **49**, 4176 (1994)] reports the first experimental observation of a second-order Young's double-slit pattern.

[4] D. N. Klyshko, Phys. Lett. A **128**, 133 (1988); **132**, 299 (1988); *Photon and Nonlinear Optics* (Gordon and Breach Science, New York, 1988).

[5] J. P. Dowling and G. J. Milburn, e-print quant-ph/0206091; A. Migdall, Phys. Today **52**(1), 41 (1999).

[6] A. N. Boto, P. Kok, D. S. Abrams, S. L. Braunstein, C. P. Williams, and J. P. Dowling, Phys. Rev. Lett. **85**, 2733 (2000).

[7] M. D'Angelo, M. V. Chekhova, and Y. Shih, Phys. Rev. Lett. **87**, 013602 (2001).

[8] A. Einstein, B. Podolsky, and N. Rosen, Phys. Rev. **47**, 777 (1935).

[9] K. R. Popper, *Quantum Theory and the Schism in Physics* (Hutchinson, London, 1983); K. R. Popper, in *Open Questions in Quantum Physics*, edited by G. Tarozzi and A. van der Merwe (Reidel, Dordrecht, 1985); K. R. Popper, in *Determinism in Physics*, edited by E. I. Bitsakis and N. Tambakis (Gutenberg, Athens, 1985).

[10] Y.-H. Kim and Y. H. Shih, Found. Phys. **29**, 1849 (1999).

[11] M. D'Angelo, Y. H. Kim, S. P. Kulik, and Y. Shih, Phys. Rev. Lett. **92**, 233601 (2004).

[12] D. N. Klyshko, *Photon and Nonlinear Optics* (Gordon and Breach Science, New York, 1988).

[13] R. S. Bennink, S. J. Bentley, and R. W. Boyd, Phys. Rev. Lett.

89, 113601 (2002).
[14] M. D'Angelo and Y. H. Shih, e-print quant-ph/0302146.
[15] M. H. Rubin, e-print quant-ph/0303188.
[16] A. Gatti, E. Brambilla, and L. A. Lugiato, Phys. Rev. Lett. **90**, 133603, (2003).
[17] R. S. Bennink, S. J. Bentley, R. W. Boyd, and J. C. Howell, Phys. Rev. Lett. **92**, 033601 (2004); J. C. Howell, R. S. Bennink, S. J. Bentley, and R. W. Boyd, *ibid.* **92**, 210403 (2004).
[18] A. Gatti, E. Brambilla, M. Bache, and L. A. Lugiato, Phys. Rev. A **70**, 013802 (2004); A. Gatti, E. Brambilla, M. Bache, and L. A. Lugiato, Phys. Rev. Lett. **93**, 093602 (2004).
[19] B. E. A. Saleh, A. F. Abouraddy, A. V. Sergienko, and M. C. Teich, Phys. Rev. A **62**, 043816 (2000).
[20] K. Wang and D. Cao, Phys. Rev. A **71**, 041801 (2005); G. Bjork, J. Soderholm, and L. L. Sanchez-Soto, J. Opt. B: Quantum Semiclassical Opt. **6**, 478 (2004); J. Bogdansky, G. Bjork, and A. Karlsson, quant-ph/0407127.
[21] D. Cao, J. Xiong, and K. Wang, Phys. Rev. A **71**, 013801 (2005); Y. J. Cai and S. Y. Zhu, quant-ph/0407240.
[22] G. Scarcelli, A. Valencia, and Y. Shih, Phys. Rev. A **70**, 051802(R) (2004).
[23] A. Valencia, G. Scarcelli, M. D'Angelo, and Y. H. Shih, Phys. Rev. Lett. **94**, 063601 (2005).
[24] D. Magatti, F. Ferri, A. Gatti, M. Bache, E. Brambilla, and L. A. Lugiato, e-print quant-ph/0408021.
[25] Note that, throughout this work, we refer to classical ghost imaging effects whenever the source inserted in the setup of Fig. 4 emits *unentangled systems of photons*. In these cases the source itself is sometimes referred as classical [even though a source of photon pairs classically correlated in momentum (Sec. V) is intrinsically quantum] to emphasize its separable nature.
[26] M. D. Reid and P. D. Drummond, Phys. Rev. Lett. **60**, 2731 (1988). For a review of several nonseparability conditions proposed in literature, see V. Giovannetti, S. Mancini, D. Vitali, and P. Tombesi, Phys. Rev. A **67**, 022320 (2003).
[27] J. W. Goodman, *Introduction to Fourier Optics* (McGraw-Hill, New York, 1968).
[28] J. Kauppinen and J. Patannen, *Fourier Transforms in Spectroscopy* (Wiley-VCH, Berlin, 2001), Chap. 10.
[29] R. P. Feynman, *The Feynman Lectures on Physics* (Addison-Wesley, New York, 1965), Vol. III.
[30] R. J. Glauber, Phys. Rev. **130**, 2529 (1963); **131**, 2766 (1963).
[31] H. Kogelnik, Appl. Opt. **4**, 1562 (1965).
[32] M. H. Rubin, Phys. Rev. A **54**, 5349 (1996).
[33] M. H. Rubin, D. N. Klyshko, Y. H. Shih, and A. V. Sergienko, Phys. Rev. A **50**, 5122 (1994).
[34] A. V. Burlakov, M. V. Chekhova, D. N. Klyshko, S. P. Kulik, A. N. Penin, Y. H. Shih, and D. V. Strekalov, Phys. Rev. A **56**, 3214 (1997).
[35] T. B. Pittman, D. V. Strekalov, A. Migdall, M. H. Rubin, A. V. Sergienko, and Y. H. Shih, Phys. Rev. Lett. **77**, 1917 (1996); D. V. Strekalov, T. B. Pittman, and Y. H. Shih, Phys. Rev. A **57**, 567 (1998).
[36] Y. H. Shih and A. V. Sergienko, Phys. Rev. A **50**, 2564 (1994); A. V. Sergienko, Y. H. Shih, and M. H. Rubin, J. Opt. Soc. Am. B **12**, 859 (1995); Y. Shih, IEEE J. Sel. Top. Quantum Electron. **9**, 1455 (2003).
[37] In this context it is worth emphasizing that the classical experiment realized in [13] does not achieve position-position correlation. Such an experiment measures the momentum-momentum correlation between the *focal planes of two lenses*. Therefore, the resulting pattern is not an image. No thin-lens equation exists for such a setup and, consequently, the observed pattern could not be reproduced anywhere else than between the focal planes. In fact, in later works, the authors referred to the effect discussed in [13] as a "far-field" image.
[38] G. Scarcelli, A. Valencia, and Y. Shih, Europhys. Lett. **68**, 618 (2004).
[39] R. Hanbury-Brown and R. Q. Twiss, Nature (London) **178**, 1447 (1956); R. Hanbury-Brown, *Intensity Interferometer* (Taylor & Francis, London, 1974).